

รายงานวิจัยฉบับสมบูรณ์

โครงการ การจำลองแบบของระบบไม่เชิงเส้นในชีววิทยาและการแพทย์: ทฤษฎีและการประยุกต์

Modeling of Nonlinear Systems in Biology and Medicine: Theory and Applications

โดย ศาสตราจารย์ ดร. ยงค์วิมล เลณบุรี และคณะ

กรกฎาคม 2548

รายงานวิจัยฉบับสมบูรณ์

ห้องสมุ

โครงการ การจำลองแบบของระบบไม่เชิงเส้นในชีววิทย์ โเละการแพทย์: ทฤษฎีและการประยุกต์

Modeling of Nonlinear Systems in Biology and Medicine: Theory and Applications

	ผู้วิจัย	สังกัด				
1.	ศ. ดร. ยงค์วิมล	เลณบุรี	มหาวิทยาลัยมหิดล			
2.	ศ. ดร. อิ มิง	ถัง	มหาวิทยาลัยมหิดล			
3.	รศ. ดร. เบญจวรรณ	วิวัฒนปฐพี	มหาวิทยาลัยมหิดล			
4.	รศ. ดร. มนต์ทิพย์	เทียนสุวรรณ	มหาวิทยาลัยมหิดล			
5.	ดร. ปิยะพงศ์	เนียมทรัพย์	มหาวิทยาลัยเชียงใหม่			
6.	ผศ. ดร. วรรณพงษ์	เตรียมโพธิ์	มหาวิทยาลัยมหิดล			

สนับสนุนโดย สำนักงานกองทุนสนับสนุนการวิจัย

(ความเห็นในรายงานนี้เป็นของผู้วิจัย สกว. ไม่จำเป็นต้องเห็นด้วยเสมอไป)

TABLE OF CONTENT

	Content		page no		
1.	PROJECT TIT	LE ,	1		
2.	RESEARCH TI	EAM	1		
3.	RESEARCH FIELD				
4.	BACKGROUND AND RATIONALE				
5.	PROJECT OBJ	UECTIVES «	8		
 3. 4. 6. 7. 	RESEARCH A	CTIVITIES	8		
	Subproject 1:	Dynamical Modeling of Systems in Medical Science	9		
	Subproject 2:	Mathematical Modeling of Blood Flow in the Coronary	24		
	4	Artery Bypass Grafting			
	Subproject 3:	Mathematical Modeling of Disease Transmission	57		
/	Subproject 4:	Application of Log-linear and Logistic Models to Cancer	60		
		Patients: A Case Study of the National Cancer Institute			
	Subproject 5:	Modeling and Computer Simulation in Cancer Research:	66		
		Theory and Modeling of the Growth of Tumors			
	Subproject 6:	Research on Asymptotic Stability of Difference Equations	88		
		with Delays			
7.	OVERALL OU	TPUT	94		
	7.1 Summary t	able	94		
 3. 4. 6. 	7.2 Rank promotions		95		
	7.3 Publication	95			
	7.4 Publication	98			
	7.5 Names of g	101			
8.	ADDITIONAL	COMMENTS	102		
	8.1 First annua	ıl meeting	102		
	8.2 Second and	nual meeting	103		
	8.3 The final report meeting				
9.	APPENDICES		103		
	9.1 Manuscripts of newly accepted / appeared papers				
	9.2 Announcer	ments of Special Seminars	107		

CONTRACT # RTA4580005

Final Report

REPORT PERIOD

31 July 2002 - 30 July 2005

1. PROJECT TITLE: Modeling of Nonlinear Systems in Biology and Medicine: Theory and Applications

การจำลองแบบของระบบไม่เชิงเส้นในชีววิทยาและการแพทย์: ทฤษฎีและการประยุกต์

2. RESEARCH TEAM:

Team Leader:

Prof. Yongwimon Lenbury, Ph.D. (Mathematics)

Address: Department of Mathematics, Faculty of Science, Mahidol University

Tel.: 02-644-5419 Fax: 02-644-5419 e-mail: scylb@mahidol.ac.th

Devoted Time per Week: 60 hours

Subproject 1: Dynamical Modeling of Systems in Medical Science Principal Investigator:

Prof. Yongwimon Lenbury, Ph.D. (Mathematics)

Address: Department of Mathematics, Faculty of Science, Mahidol University

Tel.: 02-644-5419 Fax: 02-644-5419 e-mail: scylb@mahidol.ac.th

Devoted Time per Week: 60 hours

Team Members:

2 University lecturers:

• Miss Pornsarp Pornsawad, M.Sc. (Applied Mathematics)

Address: Department of Mathematics, Faculty of Science, Silpakorn University

Tel.: (034) 243-428 Fax: (034) 243-428 e-mail: ppornsup@hotmail.com

Devoted Time per Week: 20 hours

Responsibility: research assistant in analysis and computer simulations.

▶ Miss Wannapa Kunphasuruang, M.Sc. (Applied Mathematics)

Address: Department of Mathematics, Faculty of Science, Silpakorn University

Tel.: (034) 243-428 Fax: (034) 243-428 e-mail: wannapa@su.ac.th

Devoted Time per Week: 25 hours

Responsibility: research assistant in analysis and computer simulations.

- 5 Ph.D. students
- 1 M.Sc. student

Expert Contacts:

- Prof. Phillip S. Crooke (Vanderbilt University, U.S.A.)
- Prof. Glenn F. Webb (Vanderbilt University, U.S.A.)

Subproject 2: Numerical Analysis of Pressure and Blood Flow in Artery Bifurcation with Surgical Reconstruction

Principal Investigator:

Assoc. Prof. Benchawan Wiwatanapataphee, Ph.D. (Mathematics)

Address: Department of Mathematics, Faculty of Science, Mahidol University

Tel.: 02-201-5345 Fax: 02-644-5419 e-mail: scbww@mahidol.ac.th

Devoted Time per Week: 30 hours

Team Members:

- 1 University lecturer:
- Dr. Mahosut Punpocha, Ph.D. (Mathematics)

Address: Department of Mathematics, Faculty of Applied Science,

King Mongkut's Institute of Technology North Bangkok

Tel.: 02-5878258 Fax: 02-5878258 e-mail: mpc@kmitnb.ac.th

Devoted Time per Week: 30 hours

Responsibility: research assistant with computational and modeling skills in Fluid Dynamics.

6 Ph.D. students

Expert Contacts:

> Dr. Permyos Ruengsakulrach (The Saint Louis Hospital, Thailand)

Prof. Yong Hong Wu (Curtin University of Technology, Australia)

Subproject 3: Mathematical Modeling of Disease Transmission Principal Investigator:

Prof. I. Ming Tang, Ph.D. (Physics)

Address: Department of Physics, Faculty of Science, Mahidol University

Tel.: 02-201-5773 Fax: 02-246-1381 e-mail: scimt@mahidol.ac.th

Devoted Time per Week: 20 hours

Team Members:

4 Ph.D. students

Expert Contacts:

Dr. Jean-Paul Gonzalas (Institutde Recherche pour Developpement, France)

Dr. Phillippe Barbazan (Institutde Recherche pour Developpement, France)

Prof. Dr. Warren Brockelmann (Conservation Biology Center)

Prof. Dr. Suthee Yoksan (Center for Vaccine Development)

Subproject 4: Application of Log-linear and Logistic Models to Cancer Patients: A Case Study of the National Cancer Institute

Principal Investigator:

Assoc. Prof. Montip Tiensuwan, Ph.D. (Applied Statistics)

Address: Department of Mathematics, Faculty of Science, Mahidol University

Tel.: 02-201-5762 Fax: 02-644-5419 e-mail: scmts@mahidol.ac.th

Devoted Time per Week: 20 hours

Team Members:

- 3 Ph.D. students
- 2 M.Sc. students

Expert Contacts:

Prof. Bimal K. Sinha (University of Maryland, Baltimore County, U.S.A.)

Subproject 5: Modeling and Computer Simulation in Cancer

Research: Theory and Modeling of the Growth of

Tumors

Principal Investigator:

Asst. Prof. Wannapong Triampo, Ph.D. (Physics)

Address: Department of Physics, Faculty of Science, Mahidol University

Tel.: 02-201-5770 Fax: 02-246-1381 e-mail: wtriampo@yahoo.com

Devoted Time per Week: 40 hours

Team Members:

5 Ph.D. students

Expert Contacts:

Prof. Timothy Newman (University of Virginia, U.S.A.)

Subproject 6: Research on Asymptotic Stability of Difference Equations with Delays

Principal Investigator:

Dr. Piyapong Niamsup, Ph.D. (Mathematics)
 Address: Department of Mathematics, Faculty of Science, Chiangmai University
 Tel.: (053) 943-327 Fax: (053) 892-280 e-mail: scipnmsp@chiangmai.ac.th
 Devoted Time per Week: 30 hours

.Team Members:

• 1 Ph.D./M.Sc. student

Expert Contacts:

> Prof. Julian J. Palmore (University of Illinois, U.S.A.))

3. RESEARCH FIELD: Mathematical Science (Modeling, Nonlinear Systems, Biomathematics).

4. BACKGROUND AND RATIONALE:

Characterization of biological systems has reached an unparalled level of interest and concentration. In order to arrive at a better fundamental understanding of life processes, it is imperative that powerful conceptual tools from mathematics and the physical sciences be applied to the frontier problems in biology. As stated in the 1996 report of the National Science Foundation (NSF) of the United States, "modeling of biological systems is evolving into an important partner of experimental work. All facets of biology, environmental, organism, cellular and molecular biology are becoming more accessible to chemical, physical and mathematical approaches".

The goals of mathematical, statistical, and computational approaches are to elucidate mechanisms for seeming disparate phenomena. The NSF report also voiced its belief in the tremendous potential of mathematical and computational approaches in leading to fundamental insights and important practical benefits in research on biological systems. "Mathematical and computational approaches have long been appreciated in physics and in the last twenty years have played an ever-increasing role in chemistry. It is our opinion, they are just coming into their own in biology".

As evidenced by the NSF report and the establishment of several research centers in biomathematics all over the world, it is clear that mathematical/computational methods which are based on fundamental physical laws, theory of nonlinear systems, empirical data analyses, and their combination, are providing a key element in biological research. These methods can provide hypotheses that let one go beyond the empirical data and be ready for constant testing for their range of validity. It is, in the opinion of this research team, our undeniable task to try to keep pace with this high speed development.

Despite its recognized relevance, the science of mathematical modeling still encounters resistance from some members of the professional field who might feel they have no need for unrealistic mathematical models. According to Novak (1991), there can be two answers to this skepticism. The first is that cellular and population interactions are highly nonlinear, and that many examples show intuition alone is a poor guide to predicting the behavior of nonlinear systems. Thus, although all good biologists and medical researchers already use theory, that theory could be more rigorously defined and more productively explored if it were expressed in mathematical form and its consequences investigated on this ground.

The second answer is to point out that even though the past two centuries have provided us with a rapidly growing catalog of organisms, as well as increasing detailed information about the interactions among them, it is still incomplete. Real advances in understanding how individual populations, or communities of interacting populations, respond to natural or artificial disturbance has come from combinations of mathematical models and experimental programs deliberately focused on population-level properties. The models, some of which are meant to contemplate specific systems in a detailed way, while others are constructed to answer larger questions in a relatively abstract fashion, have foundations on field and laboratory observations of the constituent individuals. All share the common purpose of helping to construct a broad theoretical framework within which to assemble an otherwise indigestible mass of field and laboratory data, and of helping us understand how seemingly simple properties at the level of individual organisms can give rise to surprising, and often bizarre, outcomes at the level of populations (Novak et al., 1991).

Recent scientific advances has made it now possible to analyze complex biological phenomena, including disease processes. Indeed, some of the most promising discoveries in biomedicine have resulted from the insights of investigators with strong backgrounds in physics, mathematics, and chemistry. Yet strong organizational barriers often impede efforts to bring scientists and students with training focused in the physical, mathematical, chemical, or quantitative sciences into research or graduate/postdoctoral programs in the biomedical science. This research team has been an instrument in the effort to encourage collaborations across disciplines and lower the barriers for interdisciplinary research. This is clearly reflected by the six subprojects carried out by the members of this research team.

The key role of interdisciplinary research and training perhaps is nowhere more evident than in the hot new field of "bioinformatics"—the study of how information is represented and transmitted in biological systems. In nerve cells, information is transmitted through electrical impulses which cause muscles to contract and endocrine cells to secrete hormones. Quite often, impulses are generated in high-frequency bursts, followed by periods of quiescence. This is particularly true in endocrine systems. It is believed that modulation of amplitudes and/or frequencies of these temporal hormone secretory patterns plays an important role in the regulation of receptor synthesis, internalization, and cellular functions. Therefore, Subproject 1.1 has been involved with investigating such cascade

feedback endrocrine systems in terms of the temporal secretion characteristics which exhibit time lags in their response mechanism.

Moreover, recent advances in instrumentation have made it possible to measure motions and mechanical forces with high speed and efficiency. These techniques have begun to supply data that has revived interest in cellular mechanics. It is now possible to make realistic models of bio-mechanical processes that can be related directly to experimentally observable, and controllable, parameters (Peskin and Oster, 1995). Subprojects 1.2 and 1.3, on mechanical ventilation and antibiotic models respectively, have taken advantage of these advances in experimental technology.

Furthermore, because of the ongoing revolution in computation theory and technology, we can now solve fluid dynamics problems in the three spatial dimensions and time (Ellington and Pedly, 1995). This opens up biological opportunities on many different scales and sizes (NSF report, 1996). For example, one can now perform fluid dynamics simulations of the embryonic and fetal heart at different stages of development. Such models will help to elucidate the role of fluid forces and flows in the control mechanisms of the human physiology. The research in Subproject 2. tackled the problem of blood flow simulation under variable boundary conditions. The difficulty in measuring and simulation of microscopic fluid flows and the dependence on access to large-scale scientific computing make it important that the best technology be made available to scientists on a scale sufficient to sustain this kind of research.

ç:

On the other hand, on the scale of populations, opportunities also exist for substantial advances in immunology by the use of modeling techniques. During the last decade mathematical modeling has had a major impact on research in immunology and virology (NSF report, 1996). Serious collaborations between theorists and experimentalists have provided break through discoveries. For example, in AIDS research experiments in which patients were given anti-retroviral drugs as perturbations of a nonlinear dynamical system, mathematical modeling combined with analysis of data obtained during drug clinical trials established for the first time that HIV is rapidly cleared from the body and that approximately 10 billion virus particles are produced daily (Ho et al., 1995). Such successes indicate that opportunities exist for developing realistic and useful models of many viral diseases, studied as a nonlinear problem. Subproject 3. has met this challenge by concentrating on modeling transmission of re-emerging viral diseases, such as dengue haemorrhagic fever, Japanese encephalites, malaria, West Nile virus, SARs, and Peptosprosis.

Considering all the above mentioned research activities with which this project has been involved, it is clear that crucial component of any research in modeling has to do with data analysis and statistical techniques and concepts. Biological and biochemical research is producing exponentially-growing data sets. Thus, a statistical component such as the group proposing Subprojects 4. and 5. has been an important integral unit in this research team. They have been devoted to modeling of processes which involve the progression of tumor, incorporating useful concepts in statistics and stochastic principles.

Last, but not least, mathematical analysis is needed to interpret the results of numerical simulations and modeling, as well as incorporate the insights into nonlinear models. There are fundamental limits to predictability of biologically interesting quantities since we are dealing with nonlinear systems with possible chaotic dynamics. This is the reason why theory and modeling studies should develop in parallel fashion. Additional theory of nonlinear systems should be made available as a necessary basis for modeling as well as experimental measurements, so that it becomes and iterative, interactive process, and thus the proposal of Subproject 6. It has provided us with the necessary theoretical foundation for asymptotic stability analysis of nonlinear systems with delays.

5. PROJECT OBJECTIVES:

- Develop necessary theory, techniques and tools to construct and analyze models of nonlinear systems.
- Construct appropriate models of nonlinear systems such as the hormone secretion system, mechanical ventilation, bacteria growth in the presence of antibiotics, blood flow, tumor growth, disease transmission, and other biological processes of current interest.
- 3. Analyze the models theoretically and numerically to gain insights leading to useful suggestions for control/management strategies.

6. RESEARCH ACTIVITIES:

This research team has in fact been studying, as well as those originally proposed for this project, several other biological systems which were not specifically mentioned in the proposal, yielding a lot more international publications than what has been promised. The following is the detailed description of activities and outputs of each subproject in the past 3 years.

Subproject 1: Dynamical Modeling of Systems in Medical Science

Principal Investigator: Prof. Dr. Yongwimon Lenbury

In general, mathematical models can be used to promote an understanding of the system of interest and they can be used to predict its behavior (Zahalak, 1992). An enhanced understanding can be achieved by describing a complicated phenomenon in terms of a limited number of simpler concepts. A good model thus allows insights into the relevant processes of the system. It can also enable one to assess how a system will behave in situations that cannot be experimentally validated.

It is important to note that the model must be developed to match the task. To choose a model, one must select a suitable model form, an appropriate level of model complexity, and a set of model parameters. Two general types of model form are structural models and phenomenological models. Structural models (sometimes called 'parametric' models) are based on fundamental physical properties of the system and may be most appropriate to gain insight into physiological processes. Phenomenological models (sometimes called 'empirical' or 'non-parametric' models) are based on observations of input/output relationships and may sometimes be suitable for simulation studies or control implementation.

Another concern in selecting a model is that of model complexity. In general, a model should be kept as simple as possible, i.e. its order and number of parameters should be as low as possible (Zahalak, 1992). Only those physiological effects should be considered that are relevant for the specific task.

The activities in this subproject can be categorized into 3 headings as follows.

1.1 Investigation of time lags in signaling responses in feedback cascade systems.

ŀ:

In many biological systems, information is transferred by hormonal ligands, and it is assumed that these hormone signals encode developmental and regulatory programs in mammalian organisms. Recently, it became apparent that hormone pulses contribute to this hormonal pool which modulates the responsiveness of receptors within the cell membrane by regulation of the receptor synthesis, movement within the membrane layer, coupling to signal transduction proteins and internalization.

In simple organisms, the detection of nonlinear or chaotic behavior in information transfer is associated with differentiation and proliferation. Modulation of the amplitude and/or the frequency of the hormone pulses in higher organisms is believed to be capable of modifying intracellular signaling pathways, gene expression, cell proliferation, and cellular functions. Modeling of episodic hormone secretion and identification of nonlinear

deterministic dynamics in an apparently irregular hormonal rhythm in human physiology can lead to valuable insights into the physiological linkage between functional and genetic programs of the living organisms.

Many hormone secretion systems incorporate some form of cascade mechanism into their operation. A system with a cascade mechanism is an amplification process where an initial reaction results in the generation of multiple second reactions, each of which sets off multiple third reactions, and so on.

An example of cascade processes is found in eco-systems such as in the plantherbivore-carnivore food chain. In general, the biomass and the reproductive rates of the components in the cascade increase as we proceed down the trophic levels. Another example of systems which incorporate the cascade mechanism involves the central nervous system, the hypothalamus, pituitary, and the distal hormone secretion glands.

Up to date, little attention to our knowledge has been devoted to analysis of cascade systems and the time lags in their response mechanisms. Although several workers have developed stability and oscillation theory for differential equations with delay (Hamada and Anderson, 1983; Lee and Zak, 1986; Bainov, 1991; and Hennet and Tarbouriech, 1997), they are concerned mainly with second order systems most of which are linear. In 1995, Campbell et al. analyzed a second-order, nonlinear delay-differential equation with negative feedback, dealing with existence for limit cycles, tori, and complex dynamics. Typically these equations take the form

$$\ddot{\mathbf{x}} + \beta \dot{\mathbf{x}} + \alpha \mathbf{x} = \mathbf{f}(\mathbf{x}_{\star}) \tag{1.1}$$

where α, β are positive constants, τ is the time delay, x, x_{τ} are the values of the controlled variable evaluated at, respectively, times t and $t - \tau$, and the function f(u) is a nonnegative, monotone decreasing function of u which describes negative feedback.

Most recently, Michiels et al. (2000) reported on the stability of perturbed delay differential equations and stabilization of nonlinear cascade systems. They studied nonlinear time delay systems of the form

$$\dot{z} = f(z, z(t-\tau)) + \Psi(z, z(t-\tau))w \tag{1.2}$$

where $z \in \Re^n$, $w \in \Re$. Investigation was carried out to find conditions under which global stability would be preserved and if not, whether semi-global stabilization was possible by reducing the size of the perturbation or modifying its shape.

We have been able to identify 3 types of delay mechanism which have been observed in biological/medical systems. The first type of delays is associated with the maturation time required before a member of the population may procreate or produce off springs. In this case, the reproduction rate r(t) at time t is a function which depends on the population density x at a time $t-\tau$; namely,

$$r(t) = f(x(t-\tau))$$

In past research works, f has been assumed to be a monotonic function. The theories concerning existence, uniqueness, persistence, or stability of a solution to the model equation usually depend on very stringent conditions on the function f. They are therefore applicable only to limited number of population models. We have investigated this type of delays as reported in Part a) below.

The second type of delays is found in cascade systems in which different components in the system possess diversified dynamics. When we move down the cascade, the components respond with drastically different speeds. A delayed response of one component to change in another component is then due to this diversified characteristics. This type of delay mechanisms can have very significant applications in the management and control of nonlinear systems in biology and medicine. We have studied a system with this type of delays as detailed in Part b) below.

The third type of delays is associated by the transport time required for a signal to travel or an increased level in one component at the peripheral region to arrive at the target organ and take its effects. For example, an injected dose of supplementary insulin may require time in transport before its increase may be felt at the target site to give rise to a reduction in the glucose level as intended. We have investigated this type of delays as detailed in Part c) below.

a) New analytical tools necessary for tackling the nonlinear system models have been developed. We have successfully proved theorems for the existence, stability, and persistance of solutions to delayed differential equations of the form

$$\dot{x}(t) = -\mu x(t) + f(x(t - \tau)) \tag{1.3}$$

which is a delayed population model capable of modelling several dynamical systems of interest in medical science, such as viral proliferation or cell divisions, etc., the rate of which is delayed by the maturation time. The function f utilized in (1.3) was assumed

٠i

in past research works to be monotone. We however allowed f to be non-monotone, and sometimes not continuous, which is more general.

The following theorems have been proved.

Theorem 1 If $f(u) < \mu u$ for all u > 0 then every solution x(t) of (1.3) converges to 0 as $t \to \infty$.

Conversely, if every solution of (1.3) converges to 0 then $f(u) < \mu u$ for all u > 0.

Theorem 2 Assume that f(x) > 0 for all x > 0 and

$$\limsup_{x \to \infty} \frac{f(x)}{x} < \mu$$

$$\liminf_{x\to 0+} \frac{f(x)}{x} > \mu$$

Then, every solution x(t) of (1.3) is persistent.

Theorem 3 Suppose that f(x) is monotonically increasing and

$$\limsup_{x \to \infty} \frac{f(x)}{x} < \mu, \tag{1.4}$$

$$\liminf_{x \to 0} \frac{f(x)}{x} > \mu.$$
(1.5)

Then, every solution x(t) of (1.3) converges to the unique \overline{x} such that $f(\overline{x}) = \overline{x}$.

Theorem 4 Suppose that f(x) is monotonically decreasing and the following system

$$a = \frac{f(b)}{\mu}$$

$$b = \frac{f(a)}{u}$$

has a unique solution $a = b = \overline{x}$. Then, every solution x(t) of (1.3) converges to \overline{x} .

Theorem 5 Suppose that $f(y_0) = \max_{x \ge 0} f(x) \le \mu y_0$. Also, (1.4) and (1.5) are assumed to

be true. Let x(t) be a persistent solution of (1.3). Then $\lim_{t\to\infty} x(t) = \overline{x}$.

Theorem 6 Suppose that (1.5) holds. Suppose, moreover, that the solution of the following system of difference equations

$$\begin{aligned} a_{n+1} &= \inf_{x \in [a_n, b_n]} \frac{f(x)}{\mu} \\ b_{n+1} &= \sup_{x \in [a_n, b_n]} \frac{f(x)}{\mu} \qquad (n = 1, 2, ...), \\ a_1 &= \inf_{x > 0} \frac{f(x)}{\mu} \qquad b_1 = \sup_{x > 0} \frac{f(x)}{\mu} \end{aligned}$$

converges to \overline{x} . Then every persistent solution of (1.3) converges to \overline{x} .

This part of our work has been published in the international journal *Mathematical*1 and Computer Modelling. Please see the paper that has appeared in Appendix # 1.1.

We have continued to work on the model (1.3) and given further stability conditions which depend on the delay τ , as well as conditions under which periodic solutions would exist. This portion of work has yielded another paper which has been accepted for publication in the *Journal of Mathematical Analysis and Applications*. Please see the full paper in Appendix # 1.2.

Further, since many systems involve many interacting components, the analysis of the system models needs more sophisticated techniques. We have therefore developed a higher order singular perturbation technique for the analysis of cascade systems involving n+3 components ($n \ge 1$). The arguments yield separation conditions on the system parameters by pivoting about the slow component of the cascade. This result has been published in *Mathematical and Computer Modelling* as can be seen in Appendix # 1.3.

Also, in many of these nonlinear system models, chaotic behavior has been often discovered which poses serious problems for control. In order to investigate how we can control such chaotic phenomena in biological systems, we considered a Komolgorov type model of cascade systems, such as food webs, with external input and removals. Applying a feedback control technique proposed by Isidori (1985), we were able to derive the rules under which chaotic solution can be counteracted and system stability or robustness may be assured. This result is published in *ScienceAsia* (appendix #1.4).

b) Modelling of bone formation has been carried out, the mathematical formulation of which was based biologically on clinical evidence observed in various reports such as that of Hock and Gera (1992), Dempster et al. (1993), Momsen and Schwarz (1997), Kong et al. (1999), Takahashi et al. (1999), Burgess et al. (1999), or Kroll (2000) amongst several others.

Firstly, since activated osteoclasts result from differentiation and activation of osteoclast precursors, we assume that a high level in osteoclast precursors is reflected in the high level of the resulting activated osteoclastic population C(t). Secondly, osteoclasts resorb bone and liberate calcium, in order to counter balance the high level of calcium in blood the rate of PTH secretion will decrease (Momsen and Schwarz, 1997). The equation for the rate of PTH secretion is then assumed to take the form

$$\frac{dP}{dt} = \frac{c_1}{k_1 + C} - d_1 P \tag{1.6}$$

where P(t) denotes the level of PTH above the basal level. The first term on the right-hand side represents the secretion rate of PTH from the parathyroid grand which decreases with the increase in the number of active osteoclastic cells C(t), c₁ and k₁ being positive constants. This accounts for the above mentioned observation that as active osteoclasts C resorb bone and liberate calcium, the rate of PTH secretion will decrease to counter balance the high level of calcium in blood. Therefore, a higher C should lead to lower PTH secretion rate. Finally, it is assumed that the hormone is removed from the system at the rate which is proportional to its current level with the removal rate constant d₁.

The dynamics of the osteoclastic population, on the other hand, can be described by the following equation

$$\frac{dC}{dt} = \frac{(c_2 + c_3 P)BC}{k_2 + P^2} - d_2 C$$
 (1.7)

where the first term on the right-hand side represents the reproduction of active osteoclasts which requires the production of osteoclast differentiation factor (ODF) and its receptor on osteoclasts (Kroll, 2000). The more C means the more ODF receptors available for the reproduction of active osteoclasts, and hence the term is taken to depend on the number of osteoclasts C at that moment in time.

Moreover, osteoclasts precursors possess RANK, a receptor of tumor necrosis factor (TNF) family that recognizes ODF through a cell-to-cell interaction with osteoblasts (Kong et al., 1999; Takahashi et al., 1999; Burgess et al.,1999; Kroll, 2000), hence the rate of reproduction is taken to depend also on the number of active osteoblastic cells B(t) at any time t. Based on the well founded theory on mathematical modeling and population dynamics known as the law of mass action (Leah, 1988), when an event occurs through cell-to-cell interaction of the two populations involved, the rate may then be assumed to

vary as their product, provided that the event occurs randomly. However, the rate of reproduction of C increases with the increase in the level of PTH (Dempster et al., 1993; Weryha and Leclere, 1995). On the other hand, it has been clinically observed (Kroll, 2000) that as PTH level increases further, it begins to inhibit osteoclastic reproduction, and hence the saturation expression $(c_2 + c_3 P)/(k_2 + P^2)$ is assumed for the stimulating effect of PTH, where c_2, c_3 , and k_2 are positive constants.

Thus, without any active osteoclasts or osteoblasts (C = 0, B = 0), the reproductive rate of C should vanish. On the other hand, C will be produced at the rate which varies directly as the product BC, by the law of mass actions mentioned before, with the variation constant c_2/k_2 at vanishing P. With PTH mediation, however, this variation parameter increases initially with increasing P but decreases when P becomes too high according to the saturation function utilized in Eq. (1.7), where c_3 is a measure of how late the inhibition effect will set in.

Finally, the dynamics of the active osteoblastic population B(t) can be described by the following equation

÷į

$$\frac{dB}{dt} = c_4 P - \frac{c_5 PB}{k_1} + P - d_3 B \tag{1.8}$$

where c_4 is the specific rate at which PTH stimulates reproduction of active osteoblasts (Brown, 1991; Isogai et al., 1996), while the second term on the right-hand side of Eq. (1.8) accounts for the clinically observed inhibition of osteoblastic differentiation due to the PTH (Kroll, 2000). PTH stimulates osteoblast differentiation in immature osteoblasts but inhibits it in more mature cells (Isogai et al., 1996), through the process of down-regulation of the PTH receptors on osteoblasts. IL-6, a cytokine produced by osteoblasts, enhances the anti-proliferative effects of PTH by suppressing the PTH-induced Ca^{2+} transients in addition to the down-regulation of the PTH receptor caused by chronic activation of the protein kinase A signal pathway. Therefore, PTH and IL-6 produced by osteoblasts exert a receptor-mediated negative feedback on the conversion of preosteoblasts to osteoblasts (Kroll, 2000). The inhibition effect is assumed here to take the form of the Holling type response function $c_5P/(k_3 + P)$ which means that there should be no such inhibition if B or P vanishes. The inhibition term $c_5PB/(k_3 + P)$ then tends to c_5B at high PTH level, so that the osteoblastic formation is predominantly stimulated positively by PTH according to

the first term c_4P in Eq. (1.4) at higher levels of this hormone. This is consistent with observed clinical data reported by both Tam et al. (1982) and Hock and Gera (1992). The parameters c_5 and k_3 may then be varied to accommodate different physiological data of different individuals. The higher k_3 means the inhibition remains effective still at higher level of PTH. The last terms in Eqs. (1.6)-(1.8) are the removal rates of the three components of the remodeling process with rate constants d_1, d_2 and d_3 , respectively.

Our reference core model, therefore, consisted of Eqs. (1.6)-(1.8), possessing highly diversified nonlinear characteristics, upon which analysis and investigation were carried out in an attempt to explain several mystifying empirical observations.

A singular perturbation analysis was carried out to yield conditions under which periodic solutions can be expected. A bifurcation diagram was then constructed to identify the ranges of a system parameter which permitted chaotic hormone secretory patterns. Our theoretical results and numerical experiments conformed with observed clinical data. Moreover, investigation of the effects of estrogen supplements suggested to us that, in order to prevent severe osteoporosis, it might be possible to give estrogen supplements only for disjointed periods and not for the entire time. The effect of a high enough dose, given during a long enough period, can last for some time after the supplement has be cut off. This lagged or delayed effect, due to the diversified time responses inherent to this cascade, can last long enough to overlap with the next period of estrogen supplement. Such dosing regimen may reduce the danger of side effects due to prolonged estrogen treatment, such as cancer.

The result of this piece of research has already been accepted and appeared in *BioSystems*, an international journal with impact factor 0.736. (Please see manuscript in Appendix # 1.5)

c) Modelling of endocrine systems has been carried out by incorporating time delays into a mathematical model of the hypothalamus adrenal cortex axis, which resulted in the following system of nonlinear delay differential equations.

$$\frac{\mathrm{dR}}{\mathrm{dt}} = -\delta_1 R + \kappa_1 e^{\beta_1 (1 - A^2 (t - \tau_2))} \tag{1.9}$$

$$\frac{dA}{dt} = -\delta_2 A + \kappa_2 e^{\beta_2 (1 - C^2 (t - \tau_2))} R(t - \tau_1)$$
 (1.10)

$$\frac{dC}{dt} = -\delta_3 C + \kappa_3 A(t - \tau_2)$$
 (1.11)

where R(t), A(t), and C(t) are plasma concentrations of corticotropin releasing hormone (CRH), adrenocorticotropic hormone (ACTH), and cortisol (C), respectively, while δ_1, δ_2 , and δ_3 are the respective hormone removal rates, and κ_1, κ_2 , and κ_3 are the respective hormone secretion rate constants. β_1 and β_2 are the feedback response potencies. The feedforward response is assumed to have a delay of τ_1 due to traveling time required before the target is reached, while the feedback effect of cortisol on ACTH or ACTH on CRH is assumed to have a delay of τ_2 .

We analyzed the model system (1.9)-(1.11) by the Hopf bifurcation theory to investigate the possibility of periodic solution and chaotic dynamics. The paper on the results has been published in the *Mathematical Medicine and Biology* with impact factor 0.368. (Please see manuscript in Appendix # 1.6).

We also applied these analytical techniques to a model of Liutinizing hormone secretion system and published another paper in *Pure and Applied Chemistry* (Appendix # 1.7)

1.2 Mathematical modeling of non-invasive mechanical ventilation

ì

ł

1

;

Many forms of pressure preset ventilation have been introduced to clinical practice, each characterized by the abrupt and periodic application and release of a set level of airway pressure at the airway opening (Boysen and McGough, 1988; Stock et al., 1987, Tharatt et al., 1988).

Although numerous attempts have been made to model the behavior of the respiratory system (Ligas et al., 1990; Burke et al., 1993; Venegas et al., 1998), few have accounted for the nonlinear pressure-flow relationships which characterize biological systems. Linear approximations sometimes serve quite well, however, the frictional component of pressure loss (influenced by changes in flow regime) varies non-linearly with the flow rate (Crooke and Marini, 1993).

In 1993, Marini and Crooke developed a general mathematical model for the dynamic behavior of a single-compartment respiratory system in response to an arbitrary applied airway pressure. It provided the means to compute most ventilation and pressure variables of clinical interest from clinician-selected and patient-specific impedance parameters. A general two-compartment model was considered by Crooke et al. in 1996. In both models, clinically important outcome variables, such as tidal volume, end-expiratory

pressure, minute ventilation and mean alveolar pressure were computed for an arbitrary applied inspiratory airway pressure.

In 1993, Crooke and Marini also presented and analyzed a nonlinear mathematical model of pressure preset ventilation which accounts for the interactive behavior of inspiratory and expiratory half cycles. It comprises a set of nonlinear differential equations which incorporates a variably nonlinear relationship between the resistive component of applied pressure and flow rate. This model was compared to the linear model of pressure preset ventilation which served to link the clinical input variables of pressure level, frequency, inspiratory time fraction, and impedance with the key outcome variables of clinical interest: tidal volume, minute ventilation, mean alveolar pressure, and end-expiratory pressure. Predictive differences arise between linear and nonlinear formulations.

In 1998, dynamics of the elastic pressure-volume (Pet-V) curve were determined during a single prolonged insufflation before and after the recruitment manoeuvre by Svantesson et al. A mathematical three-segment model of the curve including a linear intermediate segment, delineated by the lower (LIP) and upper (UIP) inflection points, was used for illustration of the recorded curves. This was due to the fact that the model was based on the concept that compliance varied with volume.

Our reference mathematical model for pressure support ventilation incorporates pressure support ventilation that is applied to a single compartment lung with compliance C, inspiratory resistance R_i , and expiratory resistance R_e . The ventilator cycle is split into two parts: inspiration of duration t_i , and expiration of duration t_e . The total length of each cycle is $t_{tot} = t_i + t_e$. During inspiration, a preset pressure P_{set} is applied to the airway, and during expiration, the ventilator applies a constant pressure P_{peep} .

At any instant of time in $[0,t_{tot}]$, there is a pressure balance between applied pressures to the compartment (P_{vent}), pressures due to elastic forces ($P_{elastic}$), pressures due to resistive forces ($P_{resistive}$), and residual pressures ($P_{residual}$). The volume of the compartment, V(t), is modeled by differential equations that correspond to the pressure balances in the system:

$$P_{\text{vent}} = P_{\text{resistive}} + P_{\text{elastic}} + P_{\text{residual}}.$$
 (1.12)

During inspiration, $P_{vent} = P_{set}$ and during expiration $P_{vent} = P_{peep}$.

This part of our work has yielded one published paper to date. In the paper, a one-compartment, mathematical model for pressure controlled ventilation, incorporating volume dependent compliances, linear and nonlinear resistances, is constructed and compared with data obtained from healthy and (oleic acid) lung-injured pigs. Experimental data is used to find parameters in the mathematical model and was collected in two forms. Firstly, the P_e – V curves for healthy and lung injured pigs were constructed; this data is used to compute compliance functions for each animal. Secondly, dynamic data from pressure controlled ventilation for a variety of applied pressures is used to estimate resistance parameters in the model. The model was then compared against the collected dynamic data. The best mathematical model is the one with compliance functions of the form C(V) = a + bV, where A0 and A1 are constants obtained from the A2 curves, and the resistive pressures during inspiration change from a linear relation A3 curves, and nonlinear relation A4 where A5 where A6 is the flow into the one-compartment lung and A6 is a positive number. The form of the resistance terms in the mathematical model indicates the possible presence of gas-liquid foams in the experimental data.

The model of non-invasive mechanical ventilation which incorporates variable compliances can then be written as follows.

Inspiration

$$R_{1}\left(\frac{dV_{i1}}{dt}\right) + \frac{V_{i1}}{a_{i} + b_{i}V_{i1}} + P_{ex} = P_{set}, \ 0 \le t \le t_{i1}$$
 (1.13)

$$R_{2}\sqrt{\frac{dV_{i2}}{dt}} + \frac{V_{i2}}{a_{i} + b_{i}V_{i2}} + P_{ex} = P_{set}, \ t_{i1} \le t \le t_{i}$$
 (1.14)

Expiration

$$R_{e}\left(\frac{dV_{e}}{dt}\right) + \frac{V_{e}}{a_{e} + b_{e}V_{e}} + P_{ex} = P_{peep}, t_{i} \le t \le t_{tot}$$

$$(1.15)$$

where V_{i1}, V_{i2} , and V_e are lung volumes during inspiration period 1, period 2, and that during expiration period, respectively. R_i and R_e are the resistances; a_i, b_i, a_e , and b_e are the compliance constants; P_{ex} is the end-expiratory pressure, P_{set} the preset pressure, and P_{peep} the ventilator applied pressure. Here, we use $\varepsilon = 1$ during $0 \le t \le t_{i1}$, and $\varepsilon = \frac{1}{2}$ during $t_{i1} \le t \le t_i$, since these give the best fit to the experimental data. Also, the value of

 t_{i1} is chosen to be the time when a sharp change in the slope of the pressure-flow curve is observed.

We have determined the system parameters in the model from experimental data, then used the model to compute key ventilatory outcome variables and compared them with clinical data. The result has been published in *Mathematical Medicine and Biology* with impact factor 0.368. (Please see manuscript in Appendix # 1.8).

1.3 Mathematical modeling of bacteria growth in the presence of antibiotics

Antibiotic resistance of bacteria is a growing problem. Mathematical models have played an important part in understanding antibiotic resistance, such as the work of Ganusov et al. (2000) which elaborated a structural approach to studying the regularities of the population dynamics of unstable recombinant bacteria strain in a chemostat. The approach was based on the mathematical modelling of all distribution in a population with different numbers of plasmid copies. In another recent study, Dibdin et al. (1996) presented a mathematical model that describes penetration of an antibacteria agent into a bacteria biofilm. As well as dealing with penetration, and the consequent bacterial lysis, the model considered diffusion of the released beta-lactamases in the extra cellular space and the consequent inactivation there of further incoming antibiotic.

As observed by McGowan et al. (2001), pharmacokinetic models of infection can make an important contribution to the study of the pharmacodynamics properties of an antibacteria agent. Apart from providing data to allow for the optimization of drug dosing regimens, such models can be used to describe the effect of a drug on a bacteria population, and provide data for more-analytical studies, as well as hypothesis testing. Analysis of the model can yield information on the pharmacodynamic parameters best correlated to the chosen outcome. Pharmacokinetic models thus play a crucial role in ensuring antibiotic efficacy and in reducing the chance of resistance.

The process of treatment of bacteria infections with antibiotics involves a multitude of variables. Many factors effect the therapeutic efficacy, such as bacteria susceptibility to antibiotics, physicochemical properties of the drug product, specific properties of the infected tissue, metabolism and elimination of antibiotic, host factors, and dosing regimen. According to Nolting and Derendorf (1995), some of the central questions for addressing this problem are

- 1. What factors govern antibacterial activity?
 - 2. How can antibiotic efficacy be quantified to permit reliable comparison between different antibiotics?
- 1 3. How can efficacy of antibiotical treatment be optimized?

In the past, dosing regimens are often based on trial and error rather than on rational design. An important step in addressing the above problem is the development and analysis of a model of antibacterial activity. The most commonly used method was the utilization of the killing curves which describe the time course of the antibacteria effect in order to find the important parameters describing the killing behavior of the antibiotic over time. Although widely employed to characterize the susceptibility of a bacterium, the method does not reflect the situation in vivo, where the antibiotic concentration is subject to considerable fluctuation due to elimination and multiple dosing regimens (Mouton et al., 1997)

In order to simulate more closely the in vivo conditions, we attempt to derive a kinetic model of the dynamics of continuous flow peritoneal dialysis with single-pass flow of fresh dialysate. We thus assume an open habitat, such as a chemostat for continuous culture of microorganisms. Two strains of microorganisms compete for a single limiting resource in the presence of an inhibitor (antibiotic) to which one strain of microorganisms is sensitive and the other resistant. Let C and X be the concentrations of the resource and the inhibitor, respectively, while S and R are the respective densities of the sensitive and resistant strains. We arrive at the following system model.

$$\frac{dC}{dt} = (C_0 - C)\omega - \frac{\varepsilon_S \psi_S SC}{(1 + \gamma X_0)(k_S + C)} - \frac{\varepsilon_R \psi_R CR}{k_R + C}$$
(1.16)

$$\frac{dS}{dt} = \frac{\psi_{S}SC}{(1 + \gamma X_{0})(k_{S} + C)} - \omega S - \frac{\varepsilon_{r}RS}{k_{r} + R} - \frac{\varepsilon_{k}X_{0}S}{k_{k} + X_{0}}$$
(1.17)

$$\frac{dR}{dt} = \frac{\psi_R CR}{k_R + C} - \omega R + \frac{\varepsilon_r SR}{k_r + R}$$
 (1.18)

Application of the singular perturbation technique led us to necessary conditions for the existence of limit cycle behavior. However, we have found that the conditions may not be satisfied simultaneously since they are self contradictory. Thus, we have concluded that the system model (1.16)-(1.18) does not permit periodic solutions. In such a case, the model is deemed not suitable, since clinical data invariably shows oscillatory behavior. We have therefore considered a modification of (1.16)-(1.18) as follows.

$$\frac{dC}{dt} = (C_0 - C)\omega - \frac{\varepsilon_S \psi_S SC}{(1 + \gamma X_0)(k_S + C)} - \frac{\varepsilon_R \psi_R CR}{k_R + C}$$
(1.19)

$$\frac{dS}{dt} = \frac{\psi_s CS(r-S)}{(1+\gamma X_0)(k_s+C)} - \omega S - \frac{\varepsilon_r RS}{k_r-S} - A_4 S$$
 (1.20)

$$\frac{dR}{dt} = \frac{\psi_R CR}{k_R + C} - \omega R + \frac{\varepsilon_r SR}{k_r + S}$$
 (1.21)

so that the susceptible bacteria S is limited by the physiological environment to grow only up to the level r.

We have used experimental data supplied by Prof. John Hotchkiss at University of Minnesota and Prof. Philip S. Crooke at Vanderbilt University to support our choices of the terms utilized in the above model. The data has been collected from a culture of two separate bacteria (Methicillin Susceptible Staphylococcus Aurens (MSSA) and Methicillin Resistant Staphylococcus Aurens (MRSA)) growing in dialysis broth. The antibiotics used were amoxicllian and vancomycin (Vanco).

The model analysis by the singular perturbation technique has been completed, yielding conditions under which different dynamic behaviors may occur. We have written the paper in a form ready to be submitted for publication. Our modelling results have been interpreted in terms of bacteria-antibiotics interaction in patients receiving dialysis treatments. Although each dialysis treatment should be regarded as a batch process, a sequence of treatments, one after the other, may be modeled as a continuous process.

However, Prof. Hotchkiss and Prof. Crooke are supplying additional measurements on the gastrointestinal tract data which is more appropriate for modelling as a continuous process. We are therefore waiting on these extra data to validate our model further. The paper shall then be submitted in short order.

Table I: Plan and Actual Activity for Subproject 1.

Activity: Proposed (Months	Months	Months	Months	Months	Months
Actual	1-6	7-12	13-18	19-24	25-30	31-36
1. Carry out extensive literature						
search to select the best	\longleftrightarrow					
approach and analytical tools	ļ					
to develop and analyze the						
model.						
2. Develop new analytical tools	————					
if necessary, or modify the						
existing ones to be more]				
capable of tackling the						
systems of interest.						
3. Develop models of cascade						
systems characterized by		\longleftrightarrow				
delay in response mechanism.						
4. Develop a model of	~	>				
mechanical ventilation.		 				
5. Develop a model of bacteria				ļ		ļ Į
growth.		←		 		
6. Analyze the resulting models.			<u></u>			
: ,	:					
7. Simulate the model to		<u> </u>				
compare with experimental						
data and make model	İ					
modification, if necessary.						
8. Make clinical interpretations		4				
and conclusions.	,					

Outputs of Subproject 1

Papers appeared/accepted in international journals	8
Papers presented in international conferences	2
Ph.D. graduates	6
Master graduate	1

Subproject 2: Mathematical Modeling of Blood Flow in the Coronary Artery Bypass Grafting

Principal Investigator: Assoc. Prof. Dr. Benchawan Wiwatanapataphee

Heart acts as a pump creating the pulsatile pressure to propel blood from the heart through arteries in which pressure is around 100 mmHg to channel the blood to arterioles to capillaries. The blood is transported back to the heart through a series of vessels: capillaries to venules to veins in which pressure is around 20 mmHg. The walls of arteries consist of three layers which are the tunica externa, the tunica media and the tunica intima. The intima is the innermost layer composed of the endothelium and connective tissue. Flow in the arteries is considered as a continuum. The arterial stretches when the pressure rises during systole and it recoils when the pressure drops during diastole. When the coronary artery is affected by a stenosis, critical flow conditions occur, for example negative pressure, high shear rate at the arterial wall and wall compression, which are thought to be the significant factors in the onset of coronary heart disease. In order to understand the genesis of coronary diseases, a number of vivo using animal model and vitro experiments have been conducted. It has been established that (i) blood behaves like a viscoelastic and a shear-thinning liquid [Fung (1984), Chien et al. (1984)], (ii) blood flow is controlled by the constriction or dilation of vessel wall, (iii) high shear stress at the wall (WSS) is correlated with various degree of stenotic artery [Holme et al. (1997), Marano et al (1998)], (iv) intimal thickening and WSS are correlated in the affected vessel [Lee et al. (1998), Kraiss et al. (1991), Krams et al (1998)] and (v) when the WSS reaches a value higher than 400 dyne/cm² the endothelial surface is irreversibly damaged [Ku (1997)]. In 1998, Marano et al. estimated WSS in collared carotid arteries of rabbits. They found that the magnitudes of the wall shear rate (WSR) are 420 s^{-1} in the healthy small arteries and between 2600-15000 s^{-1} in the stenotic arteries.

Due to a difficult task of determining the critical flow conditions for both in vivo and vitro experiments, the exact mechanism involved is still not well understood. In general, mathematical modeling and numerical simulation can give better understanding of the phenomena involved in vascular diseases. Over the last 2 decades, a number of mathematical models based on Finite Element Method (FEM) have been proposed to describe the rheological behavior of blood in the stenotic arteries using 1-D to 3-D with rigid or compliant wall. The models with particular assumptions that blood acts like a Newtonian fluid with constant viscosity and vessel is rigid seem not to be satisfactory to

predict the dynamics of real pulsatile blood flow in the artery. In 1990, Mann and Tarbell used a non-Newtonian model to determine a nonlinear dependence of the viscosity of blood on the strain rate in order to study the flow of blood analog fluids in rigid curved and straight artery models. Grigioni et al (2002) investigated the wall shear stress and velocity field via the vivo experiment in unsteady vascular dynamics and proposed a non-Newtonian model for an unsteady flow in rigid pipe driven by a known oscillatory pressure gradient. Comparison to all the validated velocity points along the vessel's lumen indicates that the results of the model in a rigid pipe are not directly related to the data in vivo experiment. However, the use of mathematical models and vivo experiments in the present works allows us to understand the importance of the rheology in blood flow, at least from a qualitative point of view. Therefore, the further development of mathematical model to study blood flow is necessary. Once a satisfactory model has been generated, the benefits to the future management of human health are unlimited.

In this study, a mathematical model is developed to study steady and unsteady state blood flow through a stenotic artery with different severity. Blood is considered as a non-Newtonian fluid. Using three geometry domains of straight tube with three different sizes of stenosis: 25%, 50% and 65%. Numerical simulations based on FEM are carried out for the flow field, temperature field and shear rate in the flow channel. Dependence of the flow on the severity of stenosis has been investigated.

2.1 Numerical simulation of blood flow in a small artery channel with solid wall

This study focuses on the blood flow in stenotic artery. A mathematical model based on FEM is developed to simulate blood flow with distribution of pressure. Blood is considered as an incompressible and non-Newtonian fluid. The flow pattern with the distribution of pressure and shear rate, are computed. The results show how the blood flows through the present stenotic area. The quadratic profile is present in the flow channel except in the stenosis area. Blood speed at the throat of the stenosis is blunt, resulting in high shear rate and dropping of pressure there. Bigger size of stenosis gives bigger shear rate and higher jumping pressure in the channel, especially around the stenosis.

2.1.1 Mathematical model

·

The computational domain is considered in the lumen channel. Blood is assumed to be an incompressible fluid. The non-Newtonian model based on Carreau model is used to determine the viscosity of blood. The fluid motion is governed by the continuity

equation, Navier-Stokes equations and defined in the domain Ω which is bounded by the boundary $\partial\Omega=\partial\Omega_{\rm in}\cup\partial\Omega_{\rm wall}\cup\partial\Omega_{\rm out}$:

$$\mathbf{u}_{i,i} = \mathbf{0},\tag{2.1}$$

$$\rho \frac{\partial u_i}{\partial t} - \nabla \cdot \eta \left(u_{i,j} + u_{j,i} \right) + \rho u_j u_{i,j} + p_{,i} = F_i, \qquad (2.2)$$

where ρ denotes the blood density of 1.06g cm⁻³, u_i represents the component of velocity vector in the *i*th direction, p denotes pressure in the channel, and F is the volume force affecting the fluid. The quantity η is the blood viscosity. We here use a Carreau model for describing viscosity by the following four-parameter equation

$$\eta = \eta_m + (\eta_0 - \eta_m)[1 + (\lambda \dot{\gamma})^2]^{(n-1)/2}, \tag{2.3}$$

where $\lambda = 3.313s$, the zero shear rate viscosity $\eta_0 = 0.56 \, dyn \cdot s/cm^2$, the infinite shear rate viscosity $\eta_{\infty} = 0.0350 \, dyn \cdot s/cm^2$ and n = 0.3568.

The quantity $\dot{\gamma}$ in equation (3) represents the shear rate given by

$$\dot{\gamma} = \sqrt{\frac{1}{2}(4u_X^2 + 4v_Y^2 + 4w_Z^2 + 2(u_Y + v_X)^2 + 2(v_Z + w_Y)^2 + 2(u_Z + w_X)^2)}.$$
 (2.4)

For three-dimensional problem, the above system of equations can be manipulated to yield a closed system of four partial differential equations in terms of four coordinates and time-dependent unknown functions u_1, u_2, u_3 and p. The system, once supplemented by the initial and boundary conditions, can be solved numerically to yield the velocity field with pressure distribution and to determine the wall shear stress. In this work, we study both steady state and unsteady state flow in the stenotic tube. The boundary conditions considered for velocity field and pressure field include the Dirichlet type and the Neumann/Robin type, i.e, for i, j = 1, 2, 3

$$\begin{aligned} \boldsymbol{u}_{i} &= \overline{\boldsymbol{u}}_{i} & \partial \Omega_{in} \\ \\ \boldsymbol{u}_{i} &= 0 & \partial \Omega_{wall} \\ \\ \boldsymbol{p} &= \boldsymbol{p}_{0}, & \eta (\boldsymbol{u}_{i,i} + (\boldsymbol{u}_{j,i})^{T}) \cdot \boldsymbol{n} = 0 & \partial \Omega_{out} \end{aligned}$$

In this work, we assumed that blood flows into an artery tube with constant velocity of 20.13 cm s⁻¹ for steady state problem and flow with the pulsatile velocity for unsteady state problem. We chose a pulsatile flow rate in the right coronary artery of 65 years old patient given by Bertolotti et al (2001) [20] and assumed that blood flows out with constant pressure 1.865×10⁵ dyn/cm² or 140 mmHg.

† 2.1.2 Weak formulation

To develop the variational statement for the boundary value problem, we consider the following representation of the problem.

Find u_1, u_2, u_3 and p such that for all test functions $\hat{u}_1, \hat{u}_2, \hat{w}_3 \in H^1_{0u}(\Omega)$ and $\hat{p} \in H^1_{0p}(\Omega)$, all the Dirichlet boundary conditions for the unknown functions are satisfied and

$$(\mathbf{u}_{::},\hat{\mathbf{p}}) = 0,$$
 (2.5)

$$\left(\rho \frac{\partial u_{i}}{\partial t}, \hat{u}_{i}\right) + \left(\rho u_{j} u_{i,j}, \hat{u}_{i}\right) - \left(\left(\eta \left(u_{i,j} + u_{j,i}\right)_{,j}\right), \hat{u}_{i}\right) + \left(p_{,i}, \hat{u}_{i}\right) = (F_{i}, \hat{u}_{i}), \quad (2.6)$$

where (\cdot,\cdot) denotes the inner product on the square integrable function space $L^2(\Omega)$, $H^1(\Omega)$ is the Sobolev space $W^{1,2}(\Omega)$ with norm $\|\cdot\|_{1,2,\Omega}$, $H^1_{0q}(\Omega) = \left\{v \in H^1(\Omega) \mid v = 0 \text{ on } \partial\Omega_q\right\}$. A standard procedure is then carried out to reduce the second-order derivatives involved in the above problem into the first-order ones using integration by parts and ensuring that all integrals involved are well defined.

To find the numerical solution of the problem, we pose the variational problem into an N-dimension subspace. The computation domain Ω is discretized into a finite number of elements connected by N nodes. Let U and P denote respectively the global vectors of velocity and pressure fields with each i th entry representing the value of the corresponding unknown function at the ith node of the finite element mesh. Then, by using the Galerkin finite element formulation, we obtain the ordinary differential equations:

$$D_{u}U = 0,$$

$$M\dot{U} + A_{u}U + A_{p}P = F,$$
(2.7)

where the superposed dot represents differentiation with respect to time and all coefficient matrices are global matrices assembled from element matrices. Matrix M corresponds to the transient term, matrices A_u and D_u correspond to the advection and diffusion terms,

matrix A_p corresponds to the pressure term and vector \mathbf{F} provides forcing functions for the Navier-Stokes equations.

2.1.3 Numerical results

A test example is given here to demonstrate the validity of mathematical model. The example under consideration is a stenotic artery with a 25%, 50% or 65% stenosis as shown in Fig.2.1. The artery is modeled by a straight tube with the length of 5 cm and diameter of 0.2 cm containing stenosis in the middle part at one side of the internal wall. In this work, a spherical shape with radius of 0.15 cm was used to define the stenosed disease. We assumed that no volume force affects the fluid.

Fig. 2.2 shows the velocity vectors and streamlines of blood at stenosis in the middle part of the domain. The flow patterns and streamlines clearly outline the path of the blood and show how the blood flows through the stenosis. The maximum speed is present at throat of the stenosis as shown in Fig. 2.3. The parabolic profile of velocity is present in the upper part and lower part of the stenosis. Fig. 2.4 shows the distribution of pressure and shear rate along a longitudinal line of the artery. It indicates that pressure drops very fast and high shear rate occurs near the stenosis.

Comparing the results obtained from three tubes with 25%, 50% and 65% stenosis, blood speed profile at the throat of the stenosis in all domains is blunt. This results in high shear rate and dropping of pressure there as shown in Fig. 2.3. Bigger size of stenosis gives bigger shear rate and higher jumping pressure in the channel, especially near the stenosis.

To study the transient flow in stenotic artery, we chose the artery with 50% stenosis and used a flow rate wave form in the right coronary artery of a 65 years old patient as an inlet flow [20]. Fig. 2.5 and Fig. 2.6 show the velocity vectors and streamlines of blood along the arterial axis at time t=0, 0.3, 0.8 and t=1.2 s. Fig. 2.7 shows the distribution of pressure and shear rate along a longitudinal line of the artery at different times. The results show that the critical flow occurs at all time, especially between t=0.3 to t=0.5 s with pressure between 1.96×10^5 to 2.23×10^5 dyn/cm² and shear rate between 1.96×10^5 to 2.23×10^5 dyn/cm² and shear rate between 1.96×10^5 to 2.23×10^5 dyn/cm² and shear rate between

t(s)	0	0.1	0.2	0.3	0.4	0.5	0.6	0.7	0.8
U_{max}	32	31	70	215	200	161	117	73	63
$p_{\text{max}} \times 10^5$	1.87	1.89	1.92	2.03	1.98	1.96	1.92	1.90	1.90
$\dot{\gamma}_{max} \times 10^5$	0.19	0.23	0.63	2.5	2.23	1.69	1.13	0.63	0.53
Re	47	42	100	389	359	276	191	109	90
t(s)	0.9	1.0	1.1	1.2	1.3	1.4	1.5	1.6	1.7
U _{max}	78	102	121	125	113	91	66	47	35
$p_{max} \times 10^5$	1.91	1.93	1.94	1.54	1.93	1.91	1.90	1.89	1.88
$\dot{\gamma}_{max}\times 10^5$	0.70	0.97	1.19	1.25	1.10	0.83	0.56	0.36	0.26
Re	117	160	195	205	183	141	97	65	47

2.1.4. Conclusions

A mathematical model for simulating blood flow in stenotic artery has been constructed. The model is used to study the critical flow in stenotic artery with severity of 25%, 50% and 65%. The result shows the significant effect of the stenosis size on fluid flow, pressure field and shear rate. The quadratic profile is present in the flow channel except in the stenosis area. The blood speed at the throat of the stenosis is blunt, resulting in high shear rate and dropping of pressure there. Bigger size of stenosis gives bigger shear rate and higher jumping pressure in the channel, especially around the stenosis. For 50% stenotic artery, the critical flow occurs at all time, especially during systolic period.

It should be addressed here that blood flow in a small stenotic artery is an extremely complex phenomenon and there are still many unsolved modeling problems. The presented work focuses on blood flow in the lumen channel without the effect of the wall. Further work could be carried out to incorporate the fluid-wall interaction in a stenotic artery.

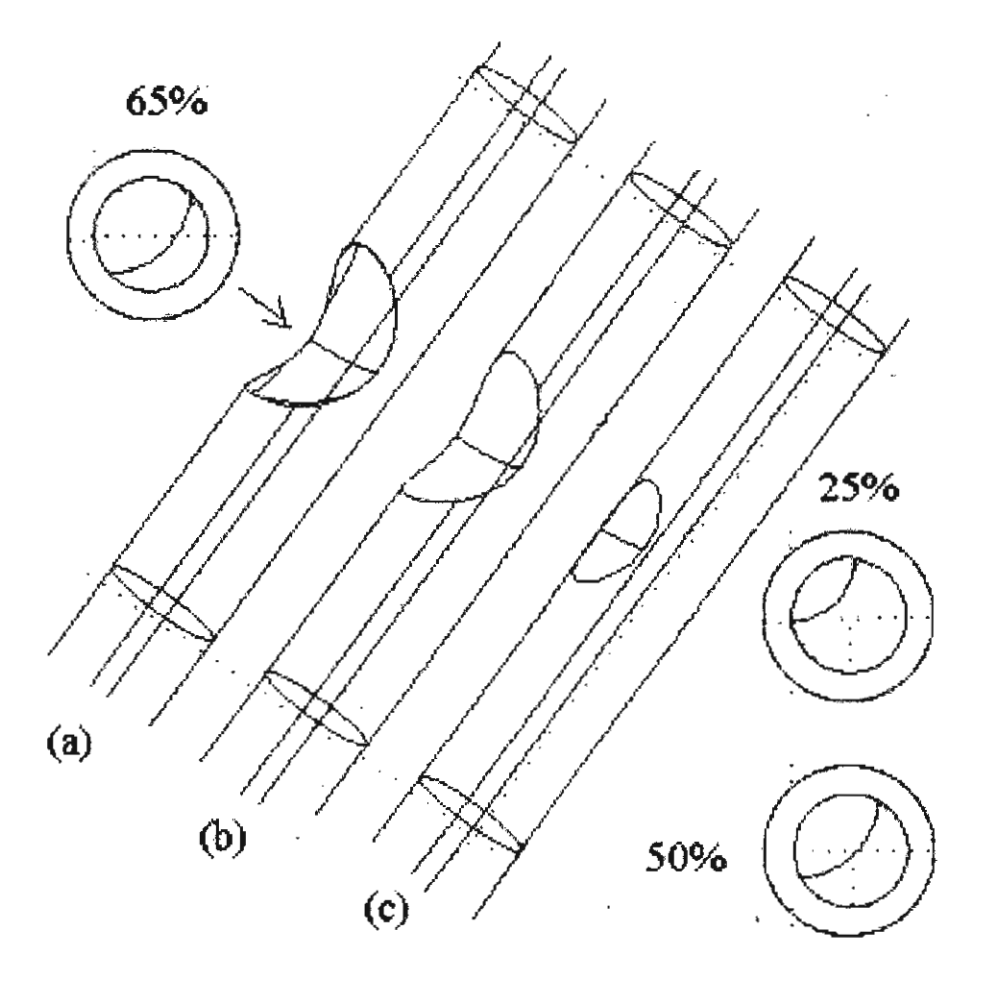


Figure 2.1 Computational domain (a) 25% stenotic tube (b) 50% stenotic tube (c) 65% stenotic tube.

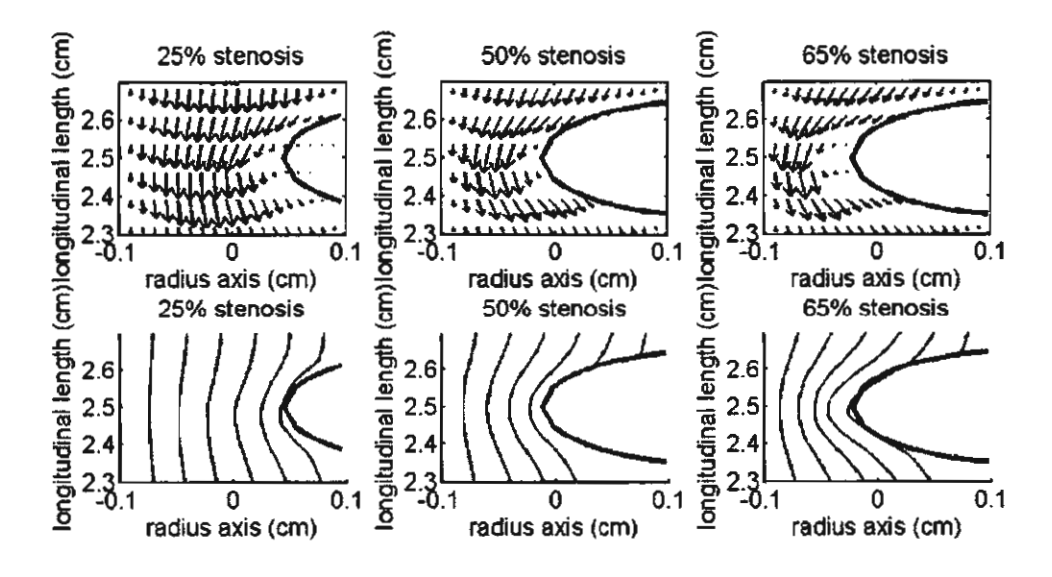


Figure 2.2 Velocity vector and streamline along the stenotic artery with different severity.

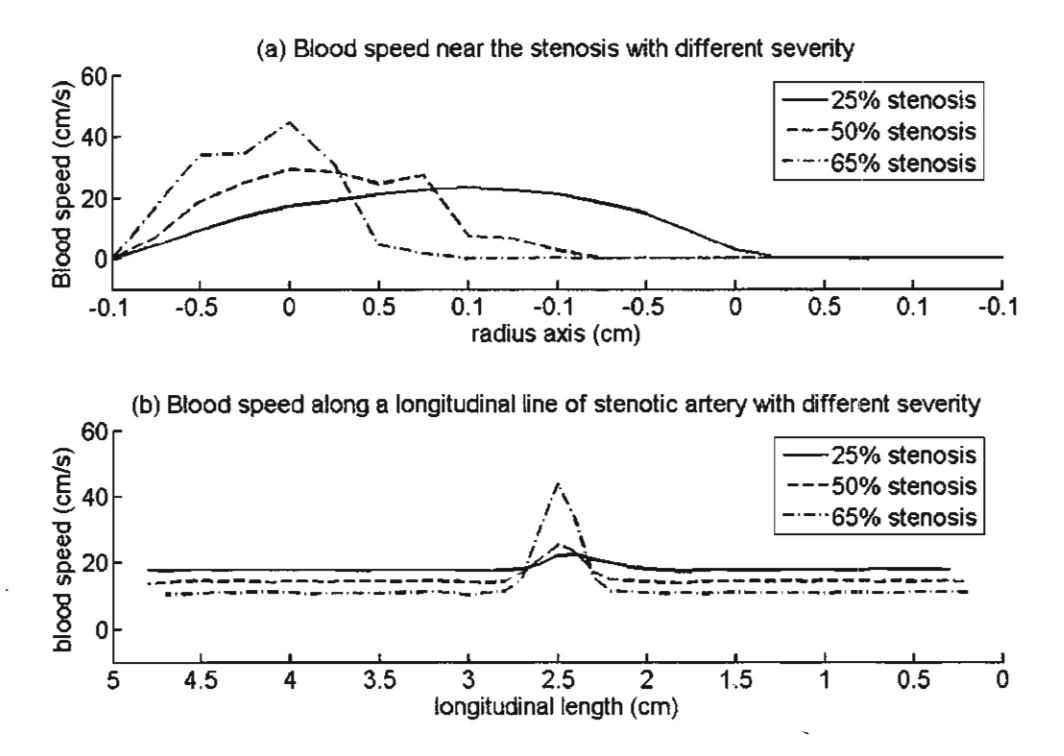


Figure 2.3 Blood speed (cm/s) at (a) mid plane of stenosis site (b) a line along the arterial axis.

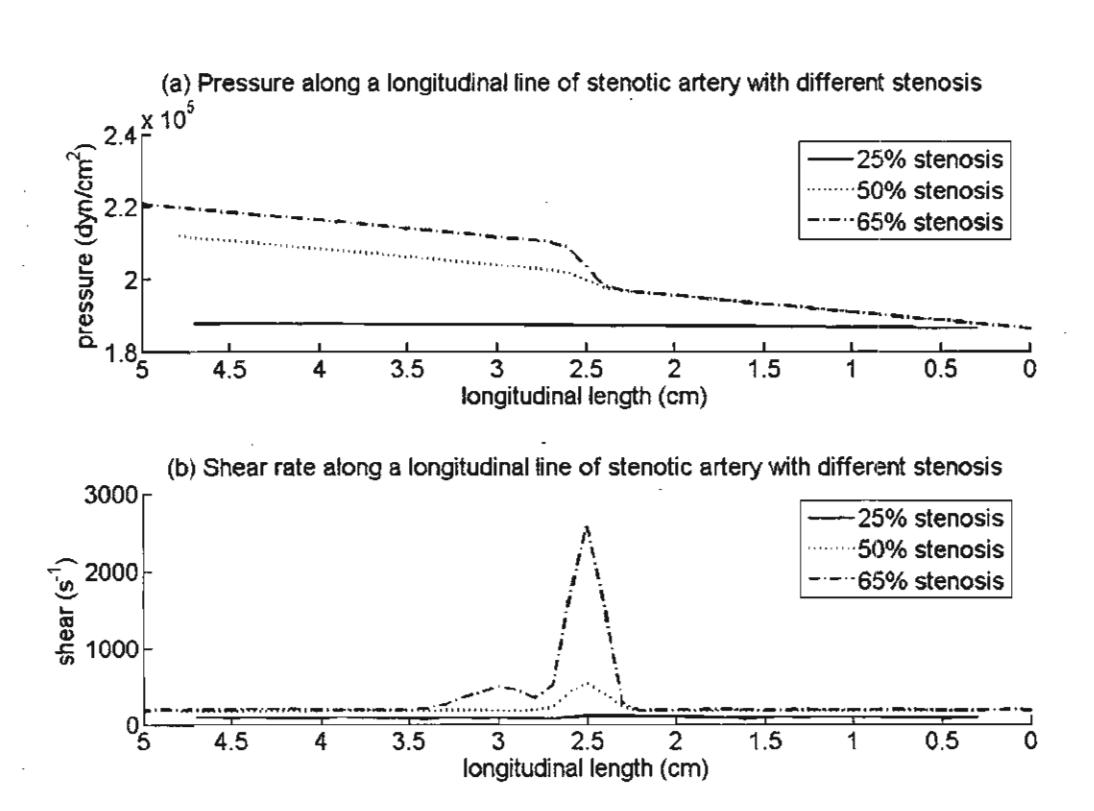


Figure 2.4 Distribution of (a) pressure (dyn/cm²) (b) shear rate (1/s) along the stenotic artery with different severity.

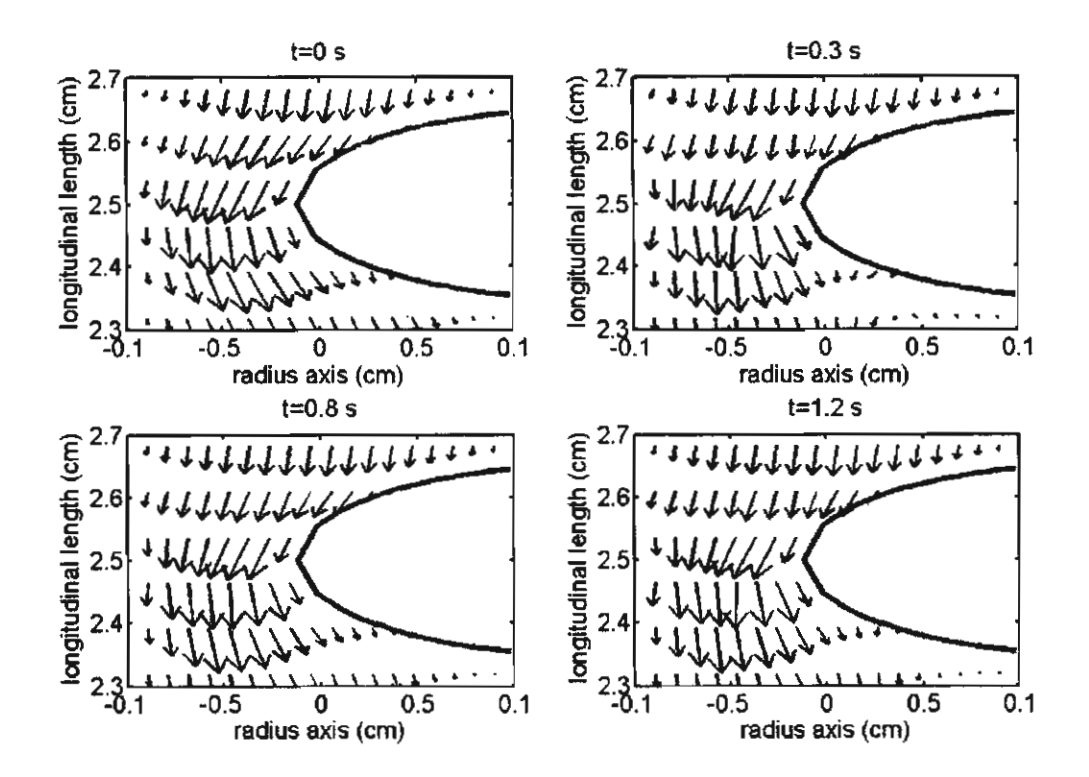


Figure 2.5 Velocity profile along a 50% stenotic artery at different time t.

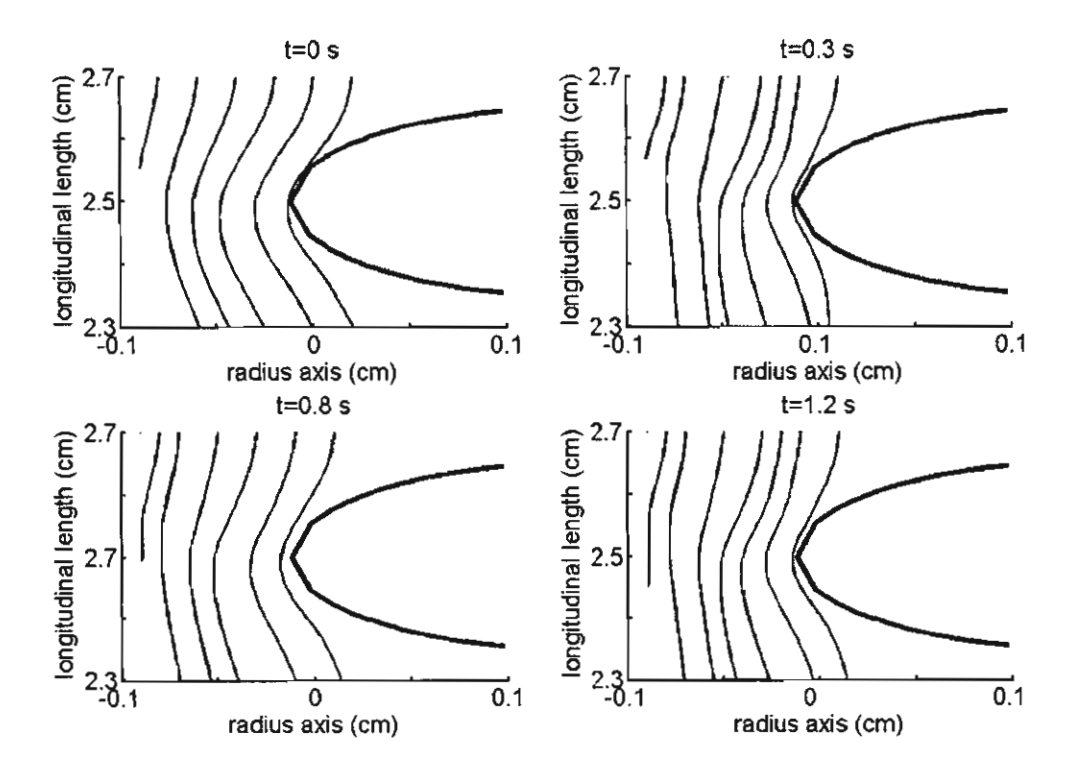


Figure 2.6 Streamline of blood flow along a 50% stenotic artery at different times t.

٤

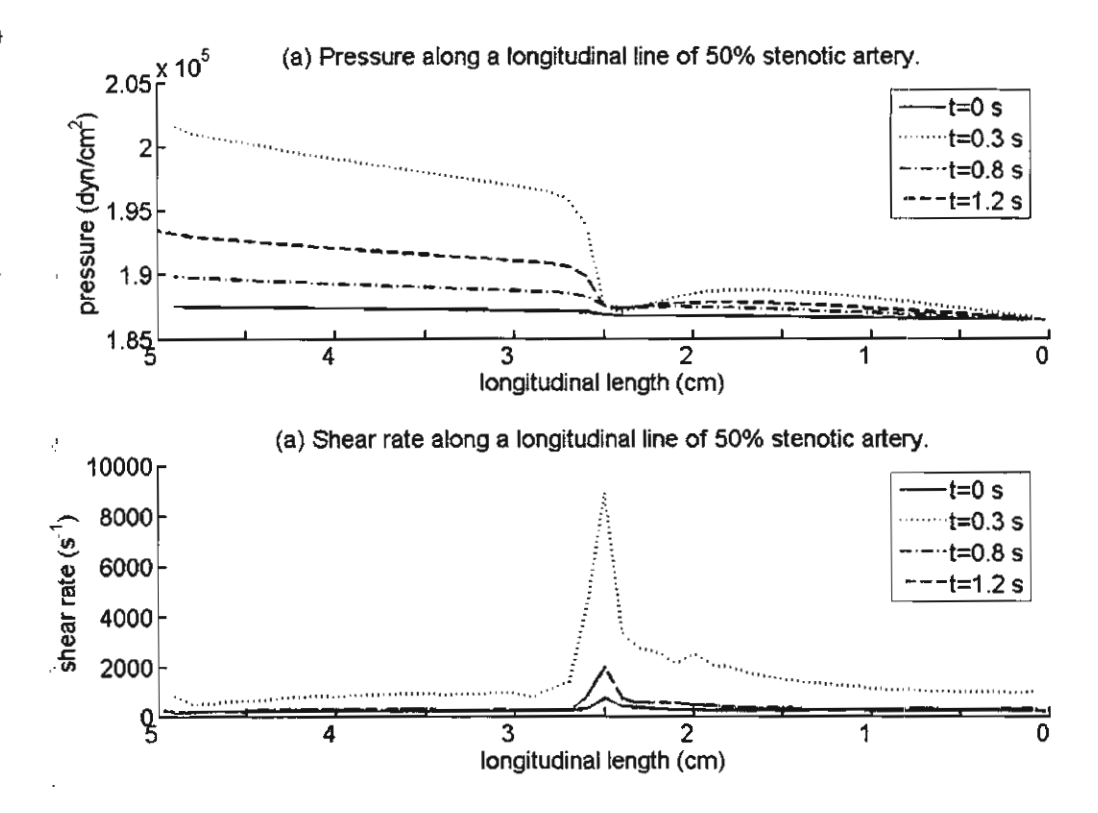


Figure 2.7 Distribution of (a) pressure (dyn/cm²) (b) shear rate (1/s) along the stenotic artery at different times t.

References

- [1] K.B. CHANDRAN, J.H. MUN, K.K.CHOI, J.S. CHEN, A.HAMILTON, A. NAGARAJ AND D.D. McPherson, A method for in-vivo analysis for regional arterial wall material property alterations with atherosclerosis: preliminary results, Medical Engineering and Physisa, 25 (2003), pp. 289-298.
- [2] F.N. VAN DE VOSSE, J. DEHART, C.H.G.A. VAN OIJEN, D. BESSEMS, T.W.M. GUNTHER, A. SEGAL, B.J.B.M. WOLTERS, J.M.A. STIJNEN AND F.P.T. BAAIJENS, Finite-element-based computational methods for cardiovascular fluid-structure interaction, Journal of Engineering Mathematics, 47 (2003), pp. 335-368.
- [3] B. CHAHBOUNE AND J.M. CROLET, Numerical simulation of the blood-wall interaction in the human left ventricle, The European Physical Journal: Applied Physics, 2 (1998), pp. 291-297.
- [4] B.M. JOHNSTON, P.R. JOHNSON, S. CORNEY, D. KILPATRICK, Non-Newtonian blood flow in human right coronary arteries: steady state simulations, Journal of Biomechanics, 37 (2004), pp. 709-720.
- [5] Y.I. CHO AND K.R. KENSEY, Effects of the non-Newtonain viscosity of blood on flows in a diseased arterial vessel. Part 1: steady flows, Biorheology, 28 (1991), pp. 241-262.

- [6] D.K. STANGEBY AND C.R. ETHIER, Coupled computational analysis of arterial LDL transport-effects of Hypertension, Journal of Biomechanical Engineering, 5:3 (2002), pp. 233-241.
- [7] P. RUENGSAKULRACH, R. SINCLAIR, M. KOMEDA, J. RAMAN, I. GORDAN, B. BUXTON, Comparative histopathology of radial artery versus internal thoracic artery and risk factors for development of intimal hypeplasia and altherosclerosis, Circulation, November 9:2 (1999), pp. 139-144.
- [8] G. KARNER AND K. PERKTOLD, Effect of endothelial injury and increased blood pressue on albumin accumulation in the arterial wall: a numerical study, Journal of Biomechanics, 33 (2000), pp. 709-715.
- [9] G.A. HOLZAPFEL, T.C> GASSER, M. STADLER, A structural model for the viscoelastic behavior of arterial walls: Continuum formulation and finite element analysis, Eoropean Journal of Mechanics A/Solids, 21 (2002), pp. 441-463.
- [10] X. ZHANG, M. FATEMI, AND J.F. GREENLEAF, Vibro-Acoustography for modal analysis of arterial vessels, IEEE, (2002), pp. 513-516.
- [11] G-T LIU, X-J WANG, B-Q AI, AND L-G LIU, Numerical study of pulsating flow through a tapered artery with stenosis, Chinese Journal of Physisc, 42:4-I (2004), pp.401-409.
- [12] F.G. BASOMBRIO, E.A. DARI, G.C. BUSCAGLIA AND R.A. FEIJOO, Numerical experiments in compleax hamodynamic flows. Non-Newtonian effects, International Journal of Computational Fluid Dynamics, 16:4 (2002), pp. 231-246.
- [13] M.R. KAAZEMPUR-MOFRAD AND C.R. ETHIER, Mass transport in an Anatomically realistic human right coronary artery, Annals of Biomedical Engineering, 29 (2001), pp. 121-127.
- [14] S. DEPARIS, M.A. FERNANDEZ, L. FORMAGGIA, F. NOBILE, Modified fixed point algorithm in fluid-structure interation, Comptes Rendus Mecanique, 331 (2003), pp. 525-530.
- [15] J-F GERBEAU, M. VIDRASCU, P. FREY, Fluid-structure interaction in blood flows on geometries based on medical imaging, Computers and Strucutres, 83 (2005), pp. 155-165.
- [16] M.A. FERNANDEZ, M. MOUBACHIR, An exact-Newton algorithm for solving fluidstructure interaction problems, Comptes Rendus Mathematique, 1336 (2003), pp. 681-686.

- [17] D. TANG, C. YANG, S. KOBAYASHI, D.N. Ku, Steady flow and wall compression in stenotic arteries: a three-dimensional thick-wall model with fluid-wall interation, Transactions of the ASME, 123 (2001), pp. 548-557.
 - [18] B.R. SIMON, M.V. KAUFMANN, M.A. MCAFEE, A.L. BALDWIN, Finite element models for arterial wall mechanics, Journal of Biomechanical Engineering, 115 (1993), pp. 489-496.
 - [19] F. ARMERO, E. LOVE, An arbitrary Lagrangian-Eulerian finite element method for finite strain plasticity, International Journal for Numerical Methods in Engineering, 57 (2003), pp. 471-508.
 - [20] C. Bertolotti, V. Deplano, J. Fuseri, P. Dupouy, Numerical and experimental methods of post-operative realistic flows in stenosed coronary artery bypasses, Journal of Biomechanics, 34 (2001), pp. 1049-1064.

2.2 Numerical study of blood flow in stenotic arteries with solid wall and permeable wall

This study focuses on the blood flow in stenotic arteries with solid wall and permeable wall. A mathematical model based on Finite element method is developed to simulate blood flow with distribution of pressure and shear rate in the lumen region and arterial wall. Blood in the lumen is considered as incompressible and non-Newtonian fluid and arterial wall is modeled as porous layer. The results show that the model with solid wall generates linear distribution of pressure along the arterial line except at the stenosis whereas the model with permeable wall gives oscillating pressure along an arterial line. High shear rate and Higher dropping pressure occurs at the stenosis. Bigger size of stenosis gives higher shear rate and higher pressure with bigger dropping pressure around the stenosis.

2.2.1 Mathematical model

١.

The computational domain consists of two regions: the arterial wall and the arterial lumen. The velocity field in the artery lumen and in the arterial wall are computed in a fully coupled manner through the use of the lumen/wall condition. Blood is assumed to be incompressible fluid and non-Newtonian fluid. The non-Newtonian model based on Carreau model is used to determine the viscosity of blood. The artery wall is assumed to be porous media with permeability of 1.0×10^{-14} . The fluid motion is governed by the

continuity equation, Navier-Stokes equations and defined in the domain $\Omega = \Omega_{\text{lumen}} \cup \Omega_{\text{wall}}$ which is bounded by the boundary $\partial \Omega = \partial \Omega_{\text{in}} \cup \partial \Omega_{\text{interface}} \cup \partial \Omega_{\text{outerwall}} \cup \partial \Omega_{\text{out}}$.

$$\nabla \cdot \mathbf{v} = 0, \tag{2.8}$$

$$-\nabla \cdot \eta \left(\nabla \mathbf{v} + (\nabla \mathbf{v})^{\mathrm{T}}\right) + \rho(\mathbf{v} \cdot \nabla)\mathbf{v} + \nabla \mathbf{p} = \mathbf{f}, \tag{2.9}$$

where ρ denotes the blood density, ${\bf v}$ represents the 3D velocity vector, ${\bf p}$ denotes pressure in the channel, and ${\bf f}$ is the volume force affecting the fluid. For this model, we assume that no volume force is affecting the fluid, so ${\bf f}=0$. The quantity η is the blood viscosity defined by the following four-parameter equation

$$\eta = \eta_{\infty} + (\eta_0 - \eta_{\infty})[1 + (\lambda \dot{\gamma})^2]^{(n-1)/2}, \tag{2.10}$$

where $\lambda=3.313s$, the zero shear rate viscosity $\eta_0=0.56 \ dyn \cdot s/cm^2$, the infinite shear rate viscosity $\eta_\infty=0.0.0345 \ dyn \cdot s/cm^2$ and n=0.3568.

The quantity $\dot{\gamma}$ in equation (3) represents the shear rate given by

$$\dot{\gamma} = \sqrt{\frac{1}{2}(4u_X^2 + 4v_Y^2 + 4w_Z^2 + 2(u_Y + v_X)^2 + 2(v_Z + w_Y)^2 + 2(u_Z + w_X)^2)}$$
 (2.11)

In arterial wall (porous domain), flow is described by the Brinkman equations according to the following.

$$\nabla \cdot \mathbf{u} = 0, \tag{2.12}$$

$$-\mu \Delta \mathbf{u} + \frac{\mu}{\kappa} \mathbf{u} + \nabla \mathbf{p} = \mathbf{g}, \tag{2.13}$$

where μ denotes viscosity in porous layer, κ is permeability, \mathbf{u} represents the 3D velocity vector, and \mathbf{g} is the volume force affecting the fluid in artery. For this model, we assume that no volume force is affecting the fluid in the artery, so $\mathbf{g} = 0$.

For three-dimensional problem, the above system of equations can be manipulated to yield a closed system of eight partial differential equations in terms of eight coordinate and time-dependent unknown functions $v_1, v_2, v_3, u_1, u_2, u_3$ and p_v, p_u . The system, once supplemented by the initial and boundary conditions, can be solved numerically to yield the velocity field with pressure distribution and to determine shear rate.

The boundary conditions considered for velocity field and pressure field include the Dirichlet type and the Neumann/Robin type, i.e, for i, j = 1, 2, 3

$$\mathbf{v} = \overline{\mathbf{v}} \quad \partial \Omega_{in} \tag{2.14}$$

$$\mathbf{p}_{\mathbf{v}} = \mathbf{p}_{0}, \quad \eta(\nabla \mathbf{v} + (\nabla \mathbf{v})^{\mathsf{T}}) \cdot \mathbf{n} = 0 \ \partial\Omega_{\text{out}}$$
 (2.15)

For steady state flow, blood speed at inlet boundary $\partial\Omega_m$ is set to the mean flow of 20.13 cm/s, and we assumed that blood flows out with constant pressure 1.865 ×10⁵ dyn/cm² or 140 mmHg at $\partial\Omega_{out}$.

At the interface between lumen and artery wall, the expression for the pressure and velocity must be continuous across the interface. We thus set

$$p_{\nu}|_{\text{wall}} = p_{u}|_{\text{wall}} \qquad \partial \Omega_{\text{interface}},$$
 (2.16)

and

١:

$$\mathbf{u}\big|_{wall} = \mathbf{v}\big|_{wall} \tag{2.17}$$

We also assumed that no slip condition is applied on the external wall. To this end, the boundary value problem for blood flow in a stenotic artery is as follows.

BVP: Find $\mathbf{v}, \mathbf{p}_{\mathbf{v}}$ and $\mathbf{u}, \mathbf{p}_{\mathbf{u}}$ such that the field equations (2.8) and (2.13) are respectively satisfied in the computational domain Ω and all boundary conditions are satisfied.

2.2.2 Weak formulation

To develop the variational statement for the boundary value problem, we consider the following representation of the problem.

Find $\mathbf{v}, \mathbf{p}_{v}$ and $\mathbf{u}^{T}, \mathbf{p}_{u}$ such that for all test function $\hat{\mathbf{v}} \in H^{1}_{0\mathbf{v}}(\Omega)$, $\hat{\mathbf{p}}_{v} \in H^{1}_{0\mathbf{p}_{u}}(\Omega)$, $\hat{\mathbf{p}}_{u} \in H^{1}_{0\mathbf{p}_{u}}(\Omega)$, all the Dirichlet boundary conditions for the unknown functions are satisfied and

$$(\nabla \mathbf{v}, \hat{\mathbf{p}}_{\mathbf{v}}) = 0, \tag{2.18}$$

$$(\rho \mathbf{v} \cdot \nabla \mathbf{v}, \hat{\mathbf{v}}) - (\nabla \cdot \eta (\nabla \mathbf{v} + (\nabla \mathbf{v})^{\mathsf{T}}), \hat{\mathbf{v}}) + (\nabla p_{\mathsf{v}}, \hat{\mathbf{v}}) = (\mathbf{f}, \hat{\mathbf{v}}), \tag{2.19}$$

$$(\nabla \mathbf{u}, \hat{\mathbf{p}}_{\mathbf{u}}) = 0, \tag{2.20}$$

$$-\mu(\Delta \mathbf{u}, \hat{\mathbf{u}}) + \frac{\mu}{\kappa}(\mathbf{u}, \hat{\mathbf{u}}), +(\nabla p_{u}, \hat{\mathbf{u}}) = (\mathbf{g}, \hat{\mathbf{u}}), \tag{2.21}$$

where (\cdot,\cdot) denotes the inner product on the square integrable function space $L^2(\Omega)$, $H^1(\Omega)$ is the Sobolev space $W^{1,2}(\Omega)$ with norm $\left|\cdot\right|_{1,2,\Omega}$, $H^1_{0q}(\Omega) = \{v\epsilon H^1(\Omega) \mid v=0 \text{ on } \partial\Omega_q\}$. A standard procedure is then carried out to reduce the second-order derivatives involved in the above problem into the first-order ones using integration by parts and ensuring that all integrals involved are well defined.

To find the numerical solution of the problem, we pose the variational problem into an N-dimension subspace. The computation domain Ω is discretized into a finite number of elements connected by N nodes. Let $\mathbf{V}, \mathbf{P}_{v}$ and $\mathbf{U}, \mathbf{P}_{u}$ denote respectively the global vectors with each i th entry representing the value of the corresponding unknown function at the ith node of the finite element mesh. Then, by using the Galerkin finite element formulation, we obtain the ordinary differential equations:

$$D_{v}V = 0,$$

$$A_{v}V + A_{pv}P_{v} = F_{v},$$
(2.22)

$$\mathbf{D}_{\mathbf{u}}\mathbf{U} = 0,$$

$$\mathbf{A}_{\mathbf{u}}\mathbf{U} + \mathbf{A}_{\mathbf{p}\mathbf{u}}\mathbf{P}_{\mathbf{u}} = \mathbf{F}_{\mathbf{u}},$$
(2.23)

where and all coefficient matrices are global matrices assembled from element matrices. Matrices A_v , A_u and D_v , D_u correspond to the advection and diffusion terms, matrix A_{pv} , A_{pu} corresponds to the pressure term and vector \mathbf{F} provides forcing functions for the Navier-Stokes equations.

2.2.3 Numerical results

A test example is given here to demonstrate the validity of mathematical model. The example under consideration is a stenotic artery with severity of 25%, 50% and 65%. The artery is modeled by a straight tube with the length of 5 cm and diameter of 0.2 cm containing stenosis in the middle part at one side of the internal wall. Wall thickness is 0.05 cm and diameter of the flow channel (lumen) is 0.2 cm. A spherical shape with radius of 0.15 cm was used to define the stenosed disease. The computational domains are shown in Section 1.

Fig. 2.8-2.10 show the velocity vectors and streamline of blood near 25%, 50% and 65% stenoses in the middle part of the solution, respectively. The flow patterns and streamlines clearly outline the path of the blood and show how the blood flows through the stenosis. The maximum speed is present at throat of the stenosis as shown in Fig. 2.11 and Fig 2.12.

Fig. 2.13 shows the distribution of pressure along a longitudinal line of stenotic artery obtained from a model with solid wall and permeable wall. It is noted that (1) for 25% stenotic artery, both models with solid wall and with permeable wall give the same pressure distribution which is a linear function along the longitudinal line of the artery; (2) blood flow in the 50% stenotic artery with solid wall generates linear distribution of pressure along an arterial line except at the stenosis where dropping pressure occurs, whereas the model with permeable wall gives the oscillating pressure along the arterial line; (3) comparison to a model with 50% stenosis, higher dropping pressure is present in the model with 65% stenosis. The model with solid wall generates linear distribution of pressure except at the stenosis whereas the model with permeable wall gives oscillating pressure along an arterial line.

Fig 2.14 shows shear rate along a longitudinal line of 25%, 50% and 65% stenotic arteries obtained from a model with solid wall and permeable wall. The results indicate that high shear rate occurs at stenosis. Comparison to a model with solid wall, it is found that (1) a model with permeable wall and 25% stenosis gives almost the same shear rate from inlet boundary to the front hill of stenosis, lower shear rate from the hill to throat of stenosis and then higher shear rate after leaving the throat of stenosis; (2) Blood flow obtained from a model with permeable wall and 50% stenosis (1) generates oscillating shear rate along the longitudinal line from inlet boundary to the back hill of stenosis, and gives the same shear rate after traveling 3 cm from inlet boundary; (3) Blood flow obtained from a model with permeable wall and 65% stenosis gives the same shear rate along the longitudinal length except the area near the stenosis where shear rate is much higher.

2.2.4. Conclusions

The results show the significant effect of permeable wall on the flow pattern of blood, especially at the stenosis area. In general, we conclude that blood speed at the throat of the stenosis is blunt, resulting in high shear rate and dropping of pressure there. Bigger size of stenosis gives bigger shear rate and higher jumping pressure in the channel, especially near the stenosis. Comparison the results obtained from the model with solid

wall and permeable wall, it is found that the model with solid wall generates linear distribution of pressure except at the stenosis and the model with permeable wall gives oscillating pressure along an arterial line. Higher dropping pressure occurs at the stenosis. Bigger size of stenosis gives bigger dropping pressure around there.

It should be addressed here that blood flow in a small stenotic artery is an extremely complex phenomenon and there are still many unsolved modeling problem. The presented work focuses on blood flow in a stenotic artery with solid wall and permeable wall. Further work could be carried out to incorporate the fluid-wall interaction in a stenotic artery when arterial wall is poroelastic material.

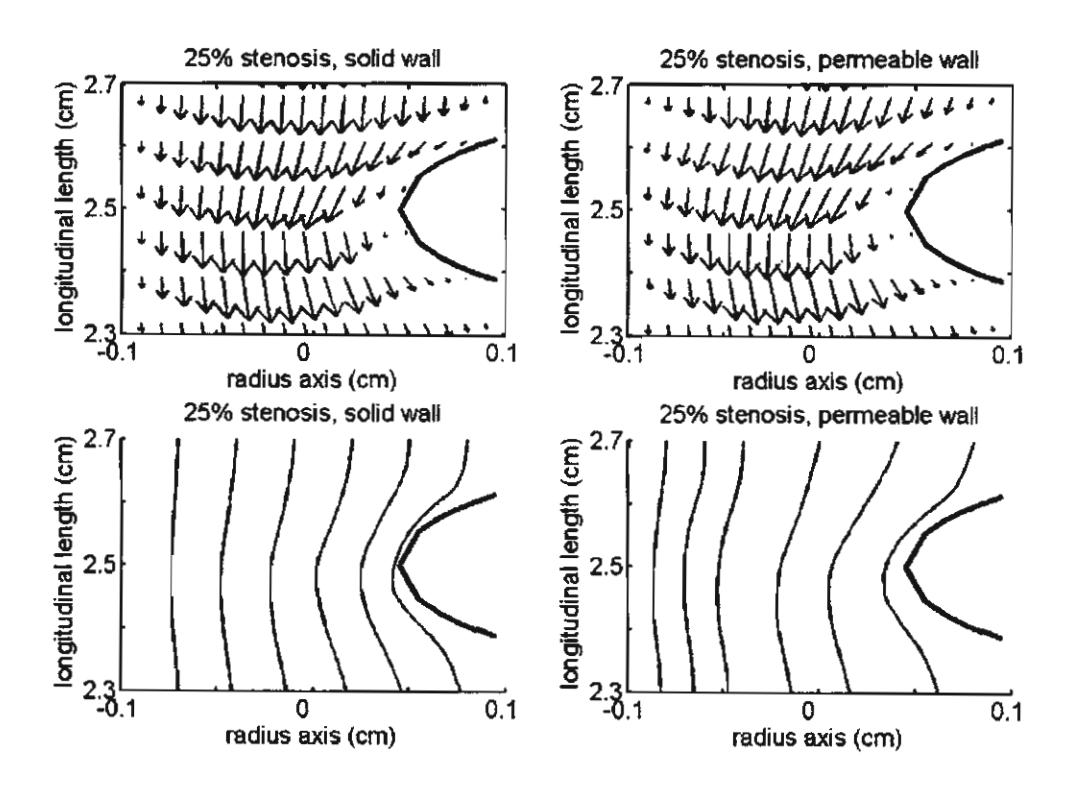


Figure 2.8 Velocity profile along 25% stenotic artery obtained from a model with solid wall and permeable wall.

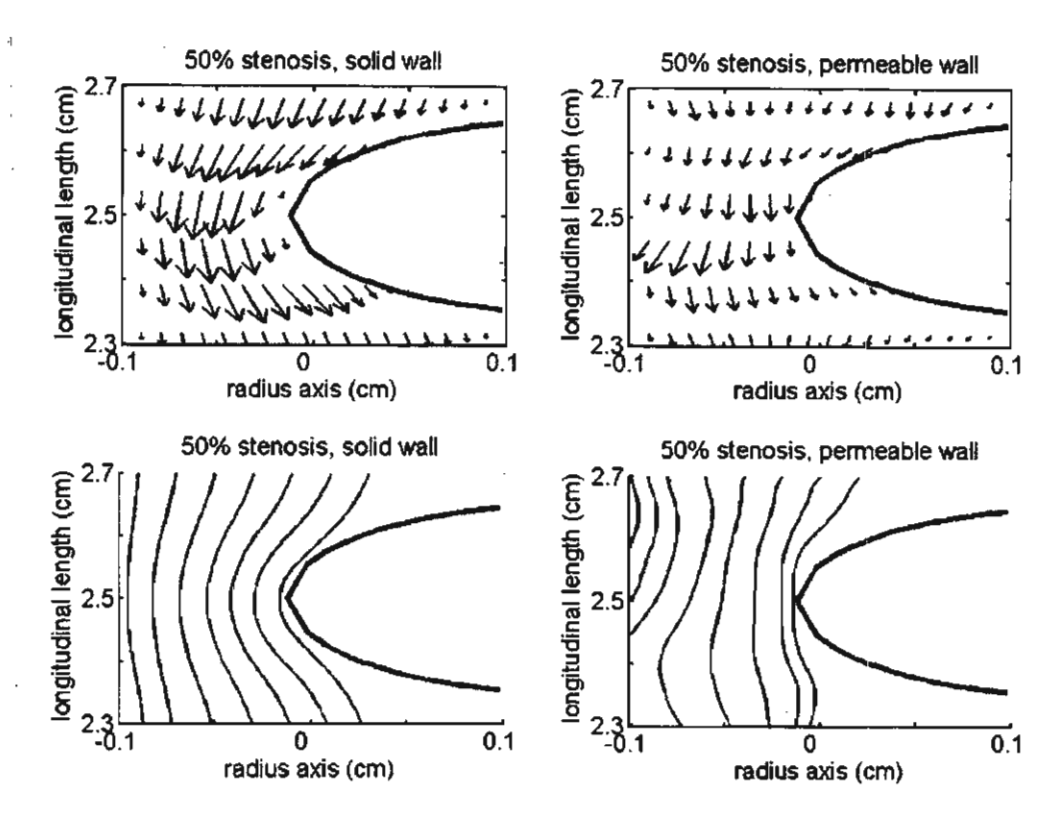


Figure 2.9 Velocity profile along 50% stenotic artery obtained from a model with solid wall and permeable wall.

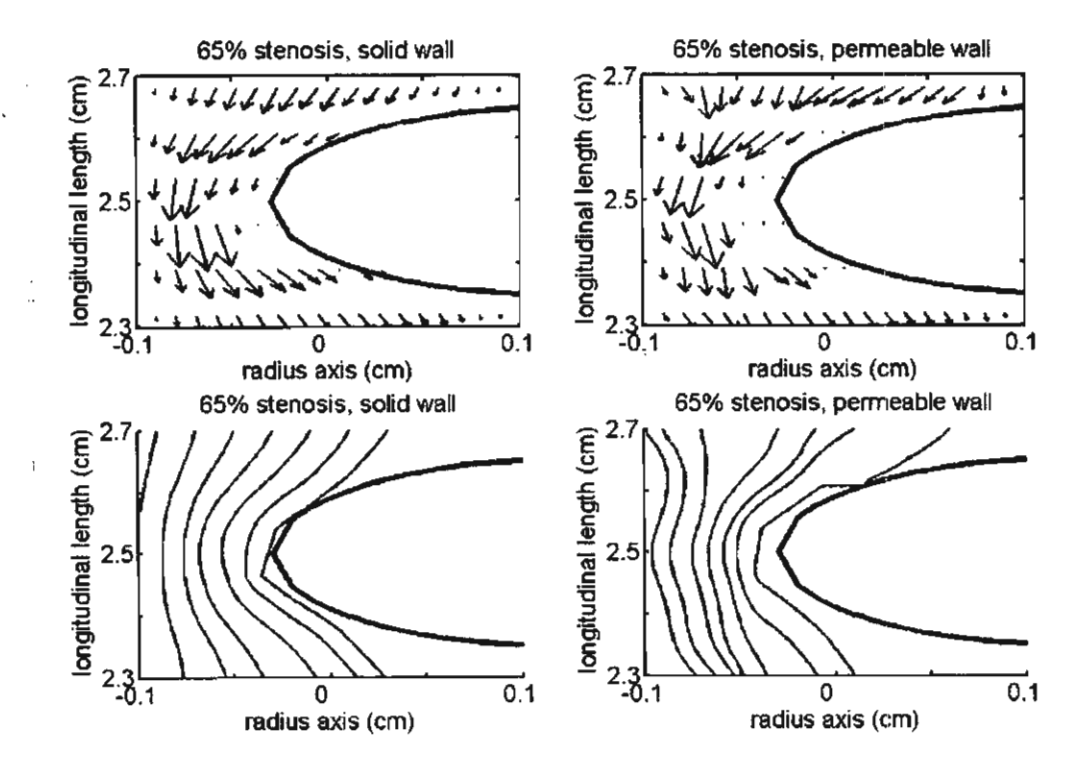


Figure 2.10 Velocity profile along 65% stenotic artery obtained from a model with solid wall and permeable wall.

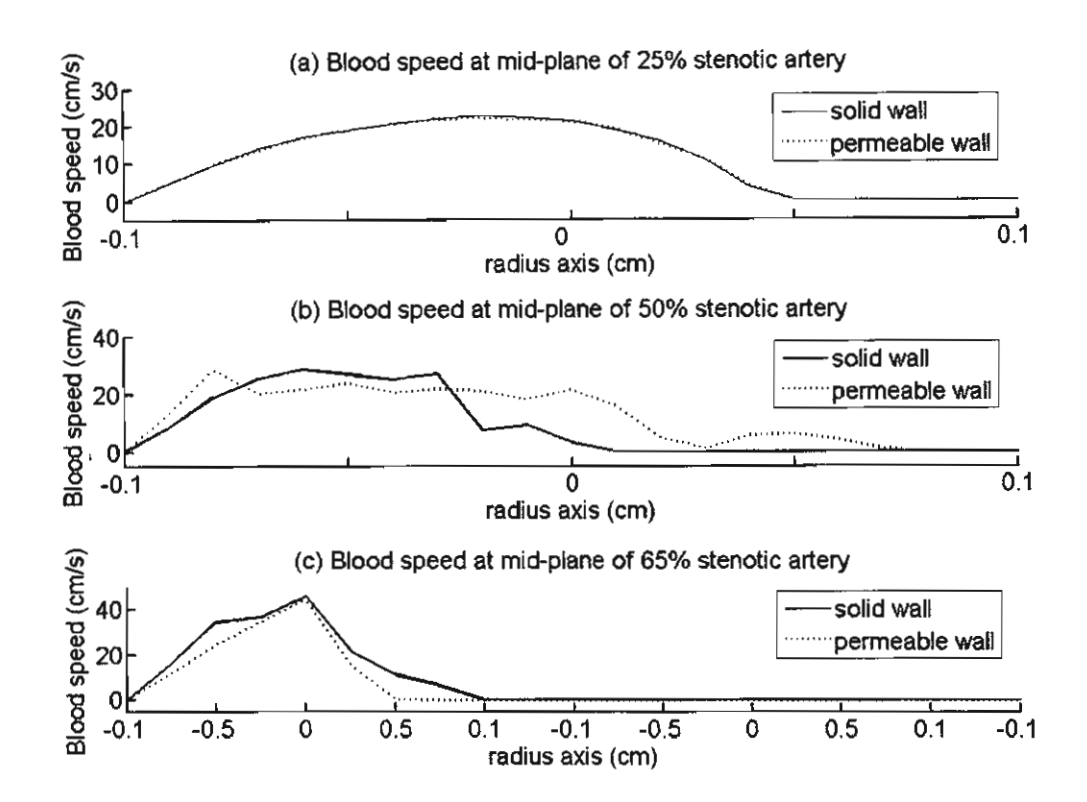


Figure 2.11 Blood speed at (a) mid plane of stenosis with different severity obtained from a model with solid wall and permeable wall.

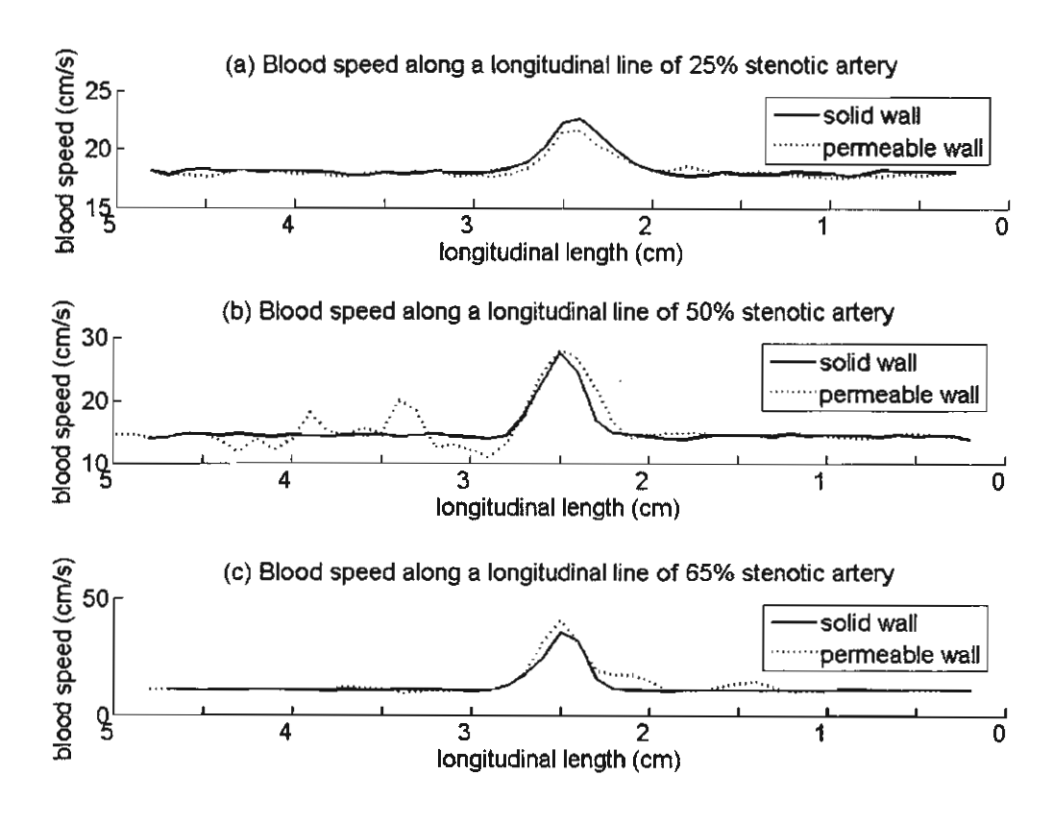


Figure 2.12 Blood speed along a longitudinal line of stenotic artery with different severity obtained from a model with solid wall and permeable wall.

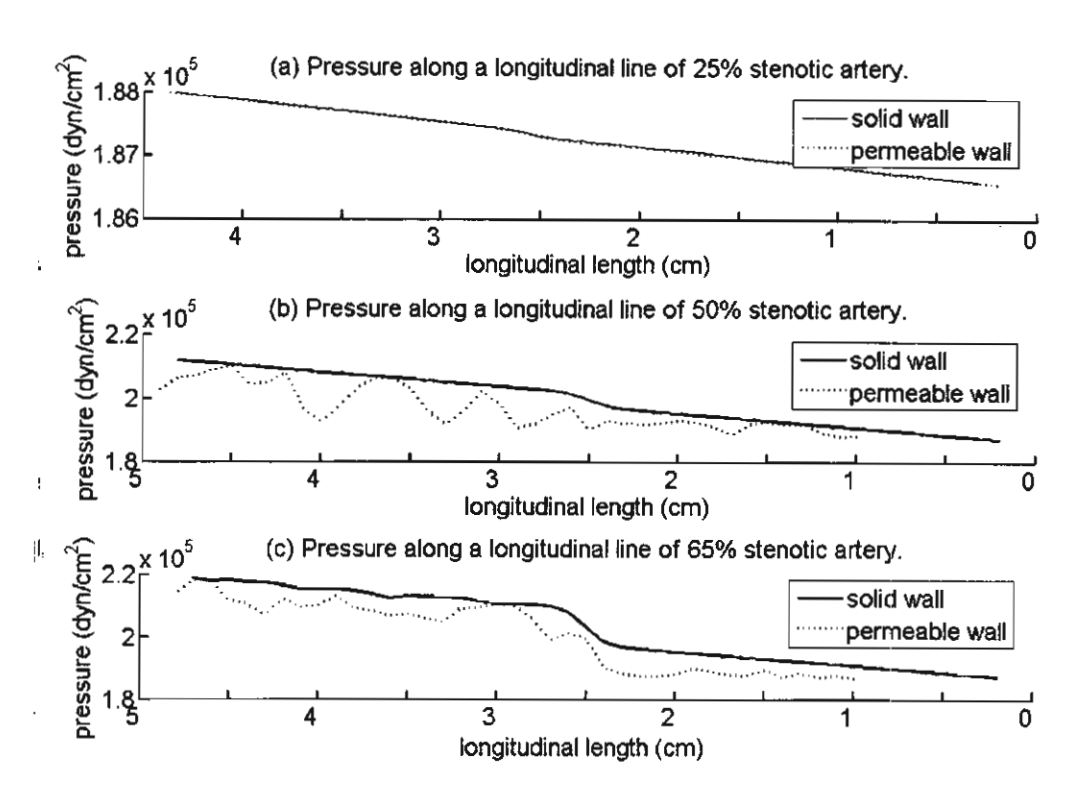


Figure 2.13 Pressure along a longitudinal line of stenotic arteries with different severity obtained from a model with solid wall and permeable wall.

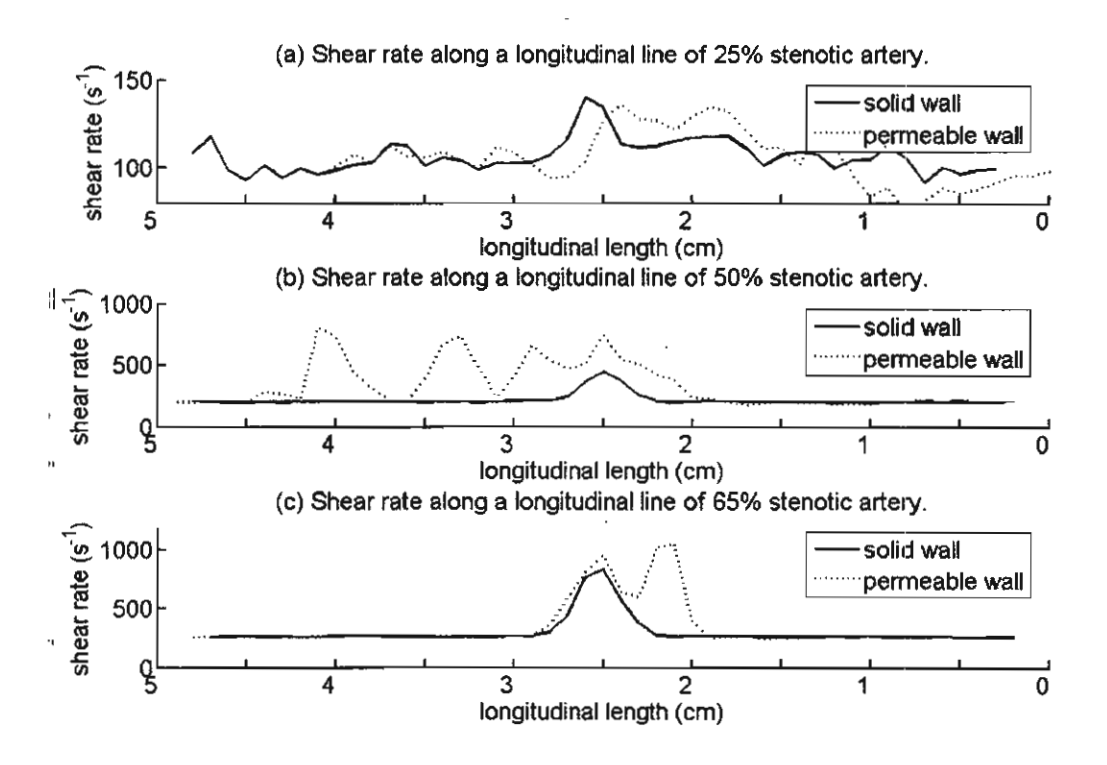


Figure 2.14 Shear rate along stenotic arteries with different severity obtained from a model with solid wall and permeable wall.

*

ĄĀ

2.3 A Numerical study of non-Newtonian blood flow in stenosed coronary artery bypass graft

It has been reported that cardiovascular disease is the leading cause of death in developed countries [1, 2]. In recent years, surgical treatments of cardiovascular diseases have been developed rapidly, and coronary artery bypass grafting (CABG) has been widely used for patients with severe coronary artery diseases. The bypass grafts are worldwide implanted each year. However, up to 25% of the grafts become occluded in one year and up to 50% occluded in ten years [3]. Intimal hyperplasia which is related to the distribution of wall shear stress (WSS) is an importance factor in failure of the coronary bypass surgery. In general, atherosclerotic lesions in the coronary arteries have been related to low and oscillating WSS [5, 4].

Another important factor in simulating blood flow is the behavior of blood. The blood is a non-Newtonian fluid with low shear rate, less than $100 \, s^{-1}$ [10]. Some numerical studies assumed the blood to be Newtonian under the assumption that the shear rate is larger than this value [11, 12, 13]. It has been known that near the center of the arteries the shear rate is small. Therefore, a non-Newtonian behavior must be taken into account in the model.

2.3.1 Mathematical model

The blood is assumed as an incompressible fluid and blood flow is laminar. The governing equations consist of the continuity equation and the Navier-Stokes equations, which can be expressed in vector notation as follows:

$$\nabla \cdot \mathbf{u} = 0, \tag{2.24}$$

$$\frac{\partial \mathbf{u}}{\partial t} + \mathbf{u} \cdot \nabla \mathbf{u} = \frac{1}{\rho} \nabla \cdot \mathbf{\sigma},\tag{2.25}$$

where \mathbf{u} and the blood velocity vector, ρ is the density of blood. σ is total stress tensor which is defined by $\sigma = -\mathbf{p}\mathbf{I} + \tau$, p is pressure, τ is the stress tensor and linearly dependent on the rate of deformation tensor \mathbf{D} with the relation $\tau = 2\eta(\dot{\gamma})\mathbf{D}$, $\mathbf{D} = \frac{1}{2}(\nabla \mathbf{u} + \nabla \mathbf{u}^T)$, η and $\dot{\gamma}$ denote the viscosity of blood and shear rate respectively. For the non-Newtonian property of blood, η depends on the shear rate $\dot{\gamma}$. The complex rheology of blood is approximated using a shear-thinning model by Carreau model.

$$\eta = \eta_{\infty} + (\eta_0 - \eta_{\infty}) [1 + (\lambda \dot{\gamma})^2]^{n-1/2}. \tag{2.26}$$

For $\dot{\gamma}$, a scalar measure of the rate of deformation tensor, $\dot{\gamma} = \sqrt{2 \text{tr}(\mathbf{D}^2)}$, η_0 and η_{∞} denote zero shear viscosity and infinite shear viscosity. The consistency index, n is the parameter between 0 and 1. The other parameters in equation (2.26) are based on Cho and Kensey [6], $\eta_{\infty} = 0.0345 \text{ g cm}^{-1} \text{ s}^{-1}$, $\eta_0 = 0.56 \text{ g cm}^{-1} \text{ s}^{-1}$, n = 0.3568, $\lambda = 3.313 \text{ s}$.

To completely define the flow problem, boundary conditions for the velocity and pressure fields must be specified. For a typical CABG system, the boundary of the computation region consists of four parts, namely the inflow surfaces of the native artery and the bypass graft, the artery wall and the outflow boundary.

On the inflow surfaces, The pulsatile velocity used in this study is shown in Figure 2.15 [7]. The flow pattern is very large during systole and small during diastole.

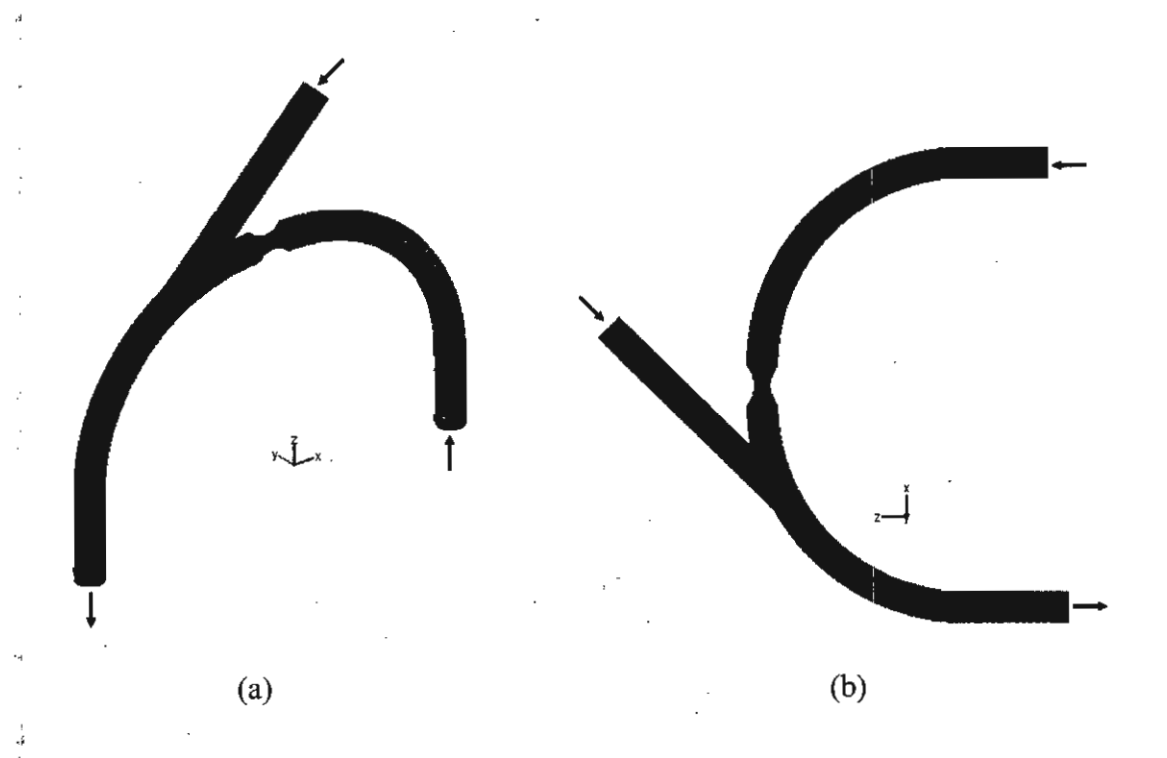


Figure 2.15 Geometry of three-dimensional 75% stenosed right coronary artery with bypass grafting model: (a) global view; (b) x-z view.

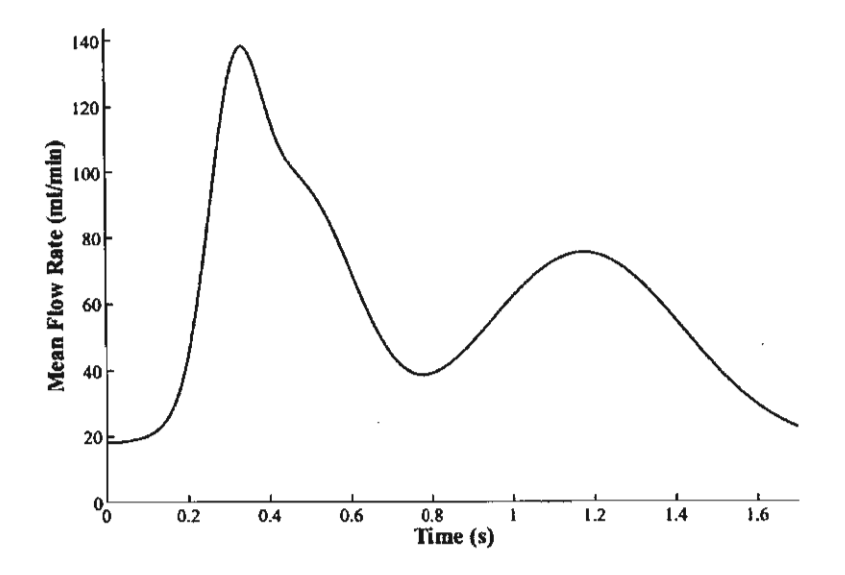


Figure 2.16 The right coronary artery volume flow rate [7].

No-slip condition is applied to the artery wall. The outflow boundary is assumed to be

$$\boldsymbol{\sigma} \cdot \mathbf{n} = p_n$$

where **n** is the unit normal vector to the outlet surface. We assume pressure at the outlet of 140 mmHg.

In summary, the fluid flow problem in CABG is governed by the following boundary value problem.

BVP: Find \mathbf{u} and \mathbf{p} such that the field equations (1) and (2) are satisfied in Ω and all boundary condition are satisfied.

2.3.2 A Numerical algorithm based on the finite element method

The variational statement corresponding to the BVP is then VBVP: Find \mathbf{u} and $\mathbf{p} \in H^1(\Omega)$ such that for all \mathbf{w}^u and $\mathbf{w}^p \in H^1(\Omega)$, all boundary conditions are satisfied and

$$(\nabla \cdot \mathbf{u}, \mathbf{w}^{\mathsf{p}}) = 0, \tag{2.27}$$

$$\left(\frac{\partial \mathbf{u}}{\partial t}, \mathbf{w}^{\mathrm{u}}\right) + \left(\mathbf{u} \cdot \nabla \mathbf{u}, \mathbf{w}^{\mathrm{u}}\right) = \frac{1}{\rho} \left(\nabla \cdot \sigma, \mathbf{w}^{\mathrm{u}}\right), \tag{2.28}$$

where (\cdot,\cdot) denotes the inner product on the square integrable function space $L^2(\Omega), H^1(\Omega)$ is the Sobolev space $W^{1,2}(\Omega)$ with norm $\|\cdot\|_{1,2,\Omega}$ and $H^1_0(\Omega) = \{v \in H^1(\Omega) \mid v = 0 \text{ on the Dirichlet type boundary}\}$.

To find the Galerkin numerical solution of the above problem, we pose the problem into a finite dimension subspace. The Galerkin finite element formulation was used in the calculation. Then, we obtained the system of ordinary differential equation,

$$C^{\mathsf{T}}U = 0,$$

$$\dot{U} + A(U)U - \overline{C}P = 0,$$
(2.29)

2.3.3 Numerical example

ij

北

Flow simulations were conducted under a typical physiological condition. The fluid properties are typical of human blood with density of 1.06 gcm⁻³ [8]. The computation region, as shown in Figure 2.15, represents the right coronary artery with 75% stenosis located at 3.95 cm from the inlet boundary. Diameter of the native artery is equal to 0.3 cm (D), and diameter of grafts is equal to 0.96×D [9]. The length of investigation is about 8.5 cm.

We simulate the blood flow through stenosis right coronary artery with 45°, 60° and 90° bypass operations in three-dimensions. The mesh as shown in Figure 2.15 consists of 27030 nodes and 15819 elements. To get flow patterns in successive cycles, each of which is divided into 280 time steps with step size 3.57 ms.

Table1: Mean/maximum velocities, pressures and mean/maximum and minimum wall shear stress

				·	
RCA with	t	U _{max}	p _{max}	WSS _{max}	$\overline{\mathrm{WSS}}_{\mathrm{min}}$
75% stenosis	(s)	(cm/s)	(mmHg)	(dyn/cm ²)	(dyn/cm ²)
	0.4	150.68	145.99	449.70	0.53
Without	0.8	47.55	141.56	113.75	0.55
bypass graft	1.2	92.91	143.38	255.98	0.79
	1.6	36.91	140.91	80.61	0.34
	0.4	154.16	147.72	442.03	1.422
With 45°	0.8	48.28	142.06	111.13	0.40
bypass graft	1.2	94.71	144.52	253.79	0.85
	1.6	37.09	141.17	82.18	0.46
	0.4	157.51	148.15	2760.47	0.00
With 60°	0.8	46.75	142.01	916.00	0.00
bypass graft	1.2	91.75	144.48	1765.31	0.00
	1.6	36.62	141.15	692.76	0.00
	0.4	183.61	147.80	520.25	0.00
With 90°	0.8	49.78	141.75	123.35	0.00
bypass graft	1.2	94.54	143.96	273.83	0.00
	1.6	38.05	141.01	87.22	0.00
			1	1	

Table 1 shows the maximum blood speed, pressures and maximum and minimum wall shear stress. Maximum speed at the throat of stenosis obtained from each domain is very high at the peak systolic. The results indicated that pressure drops along the arterial axis. Figure 2.17 shows, in x-z plane, that the retrograde flows occur along the vessel wall in the neighborhood of heel part in the native artery. Bypass graft with 45° produces the re-circulation zone in the cardiac cycle. The re-circulating jet flow tends to decrease as the anastomosis angle increases as shown in Figure 2.18.

Figures 2.19 and 2.20 show the wall shear stress along the lines A and B, respectively. The results indicate that very high WSS occurs during systole period. Figure 2.19 shows that wall shear stress at the bed of graft (line A) tends to increase after bypass operation for all graft angles. Figure 2.20 shows WSS at the toe part of the graft (line B). High WSS is present at the toe part as shown in Figure 2.20.

2.3.4 Conclusions

A mathematical model of blood flow patterns in the 75% right coronary artery bypass grafting is presented based on the Bubnov-Galerkin Finite Element formulation. The three-dimensional non-Newtonian flow is calculated. On comparing the results with other angles of bypass grafts, the ones of 45° graft angle seem to be satisfied. It can be stated that the proper choice of the diameter of the graft might improve the balance of inflow and outflow in the coronary artery. It should be addressed that to improve the accuracy of results, the effect of porous wall and wall deformation must be included. Therefore, further research work is required.

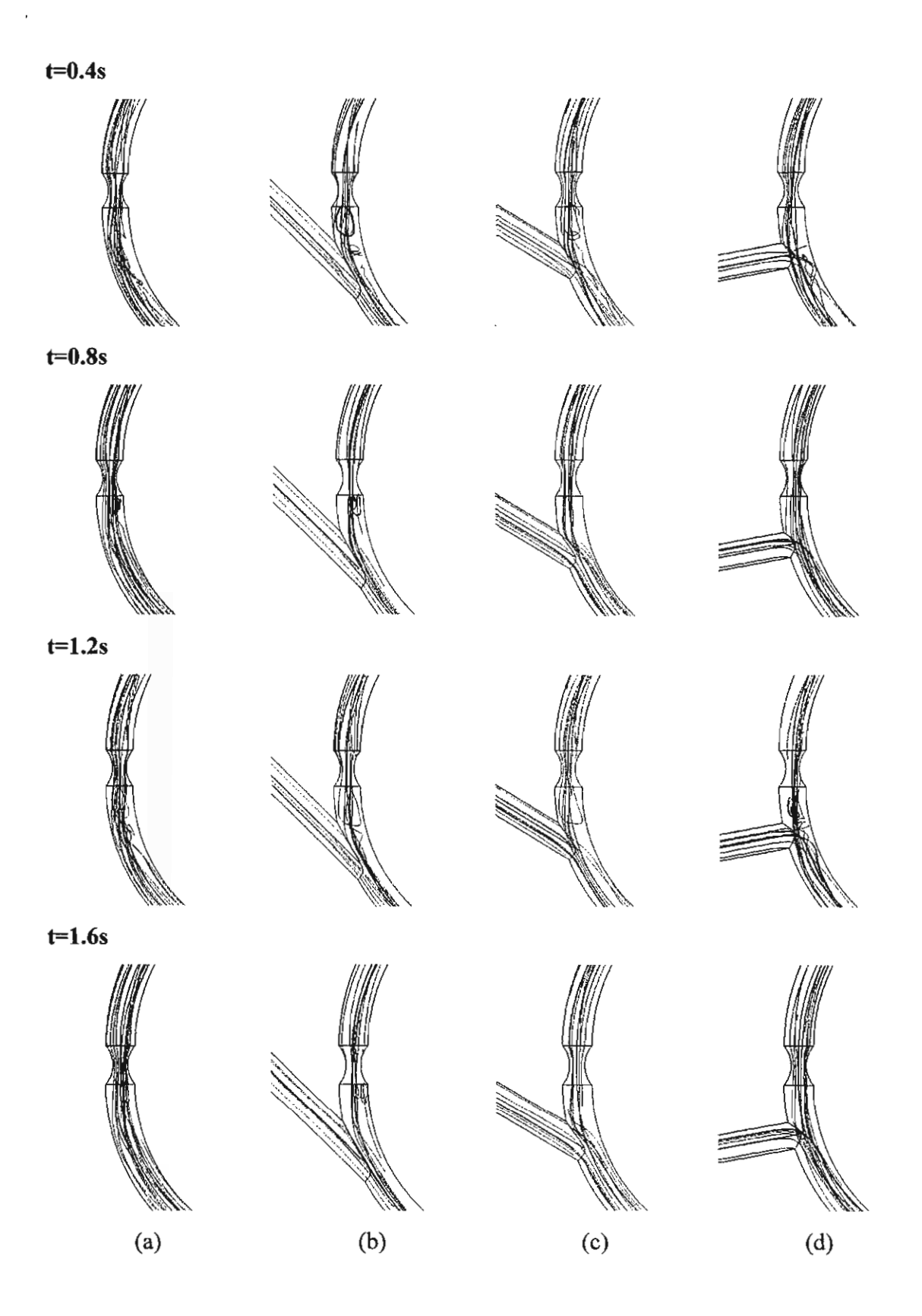


Figure 2.17 The streamline velocity field in RCA (a) without and (b)-(d) with bypass operation 45° , 60° and 90° , respectively, in x-z plane at specific times.

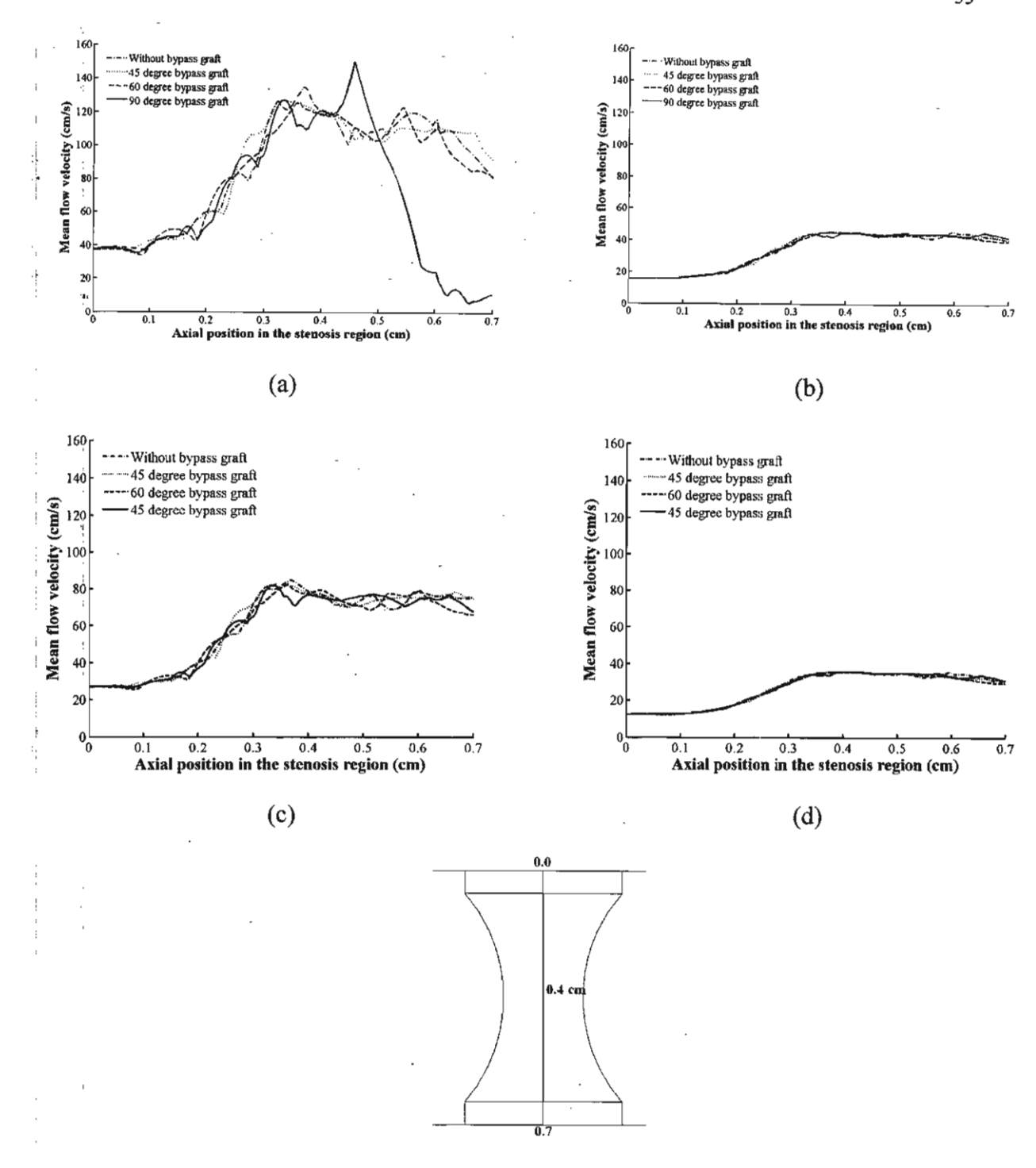


Figure 2.18 Axial distribution of mean axial velocity in the stenosis region at specific times: (a) t=0.4s, (b) t=0.8s, (c) t=1.2s and (d) t=1.6s.

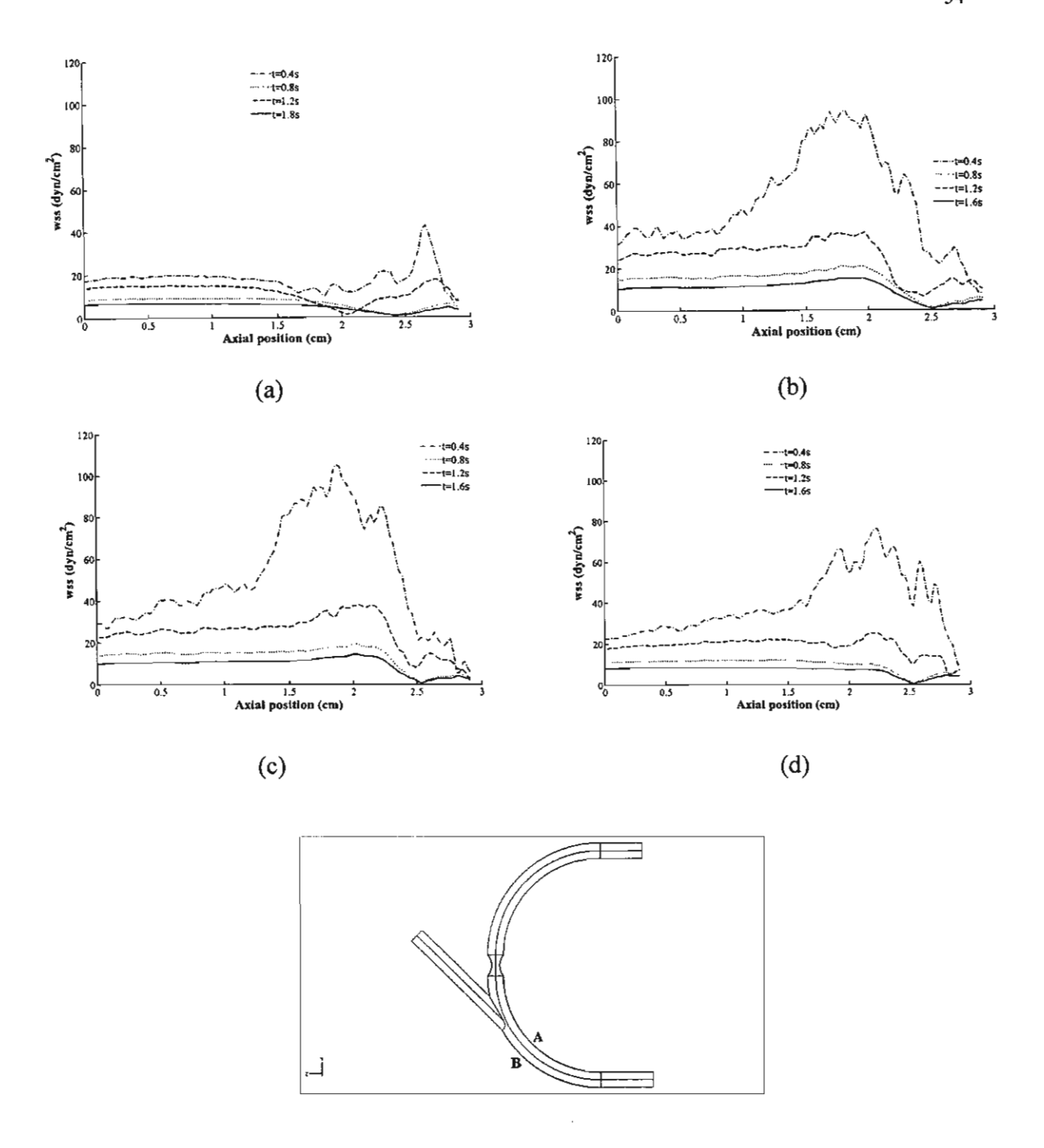


Figure 2.19 The wall shear stress evaluation along line A: (a) without bypass grafting and with bypass grafting of angles (b) 45° , (c) 60° and (d) 90° .

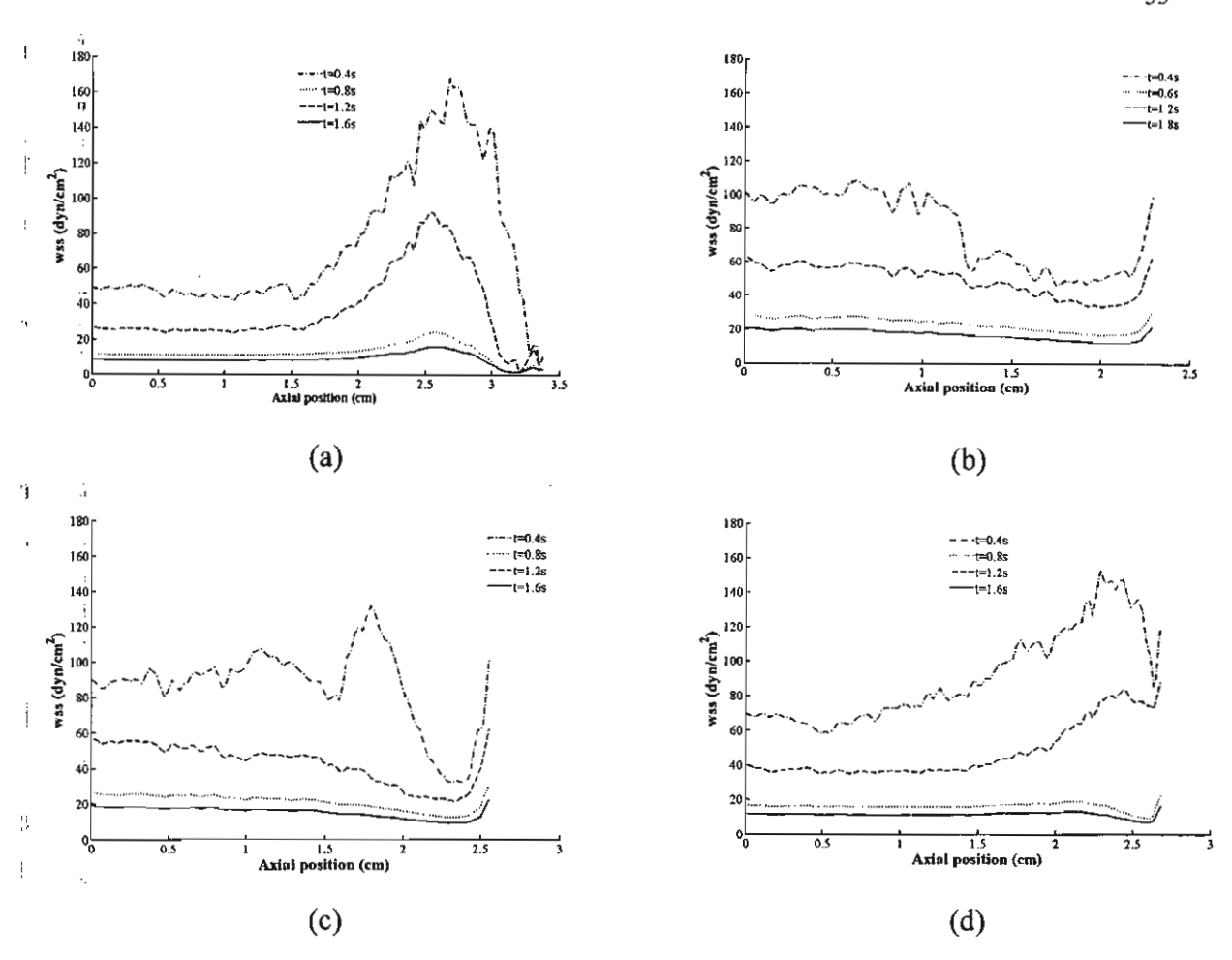


Figure 2.20 The wall shear stress evaluation along line B: (a) without bypass grafting and (b)-(d) with bypass grafting of angles 45° , 60° and 90° , respectively.

References

- [1] CARO, C.G., FITZ-GERALD, J.M., SCLIROTER, R.C, Atheroma and arterial wall shear: observation, correlation and proposal of a shear dependent mass transfer mechanism for atherogenesis, Proc. Roy. Soc. B, 177 (1971), pp. 109-159.
- [2] Organisation Mondiale de la Sante (OMS). Annual Report, 1999.
- [3] Y. PAPAHARILAOU, D.J. DOORLY, S.J. SHERWIN, The influence of out-of plane geometry on pulsatile flow within a distal end-to-side anastomosis, J Biomech, 35 (2002), pp. 1255-39.
- [4] C.R. ETHIER, D.A. STEINMAN, X. ZHANG, S.R. KARPIK, M. OJHA, Flow waveform efects on end-to-side anastomotic patterns, J Biomech, 31 (1998), pp. 609-17.
- [5] E.S. WEYDAHL, J.M. MOORE JR., Dynamic curvature strongly affects wall shear rates in a coronary artery bifercation model, J Biomech, 34 (2001), pp. 1189-96.

- [6] Y.I. Cho, K.R. Kensey, Effects of the non-Newtonian viscosity of blood on flows in a diseased arterial vessel. Part 1: steady flows, Biorheology. 28 (1991), pp. 241-262.
- [7] C. Bertolotti, V. Deplano, J. Fuseri, P. Dupouy, Numerical and experimental models of post-operative realistic flows in stenosed coronary bypasses, J Biomech, 34 (2001), pp. 1049-64.
- [8] D. TANG, C. YANG, S. KOBAYASHI, KU DN, Steady flow and wall compression in stenotic arteries: a three-dimensional thick-wall model with fluid-wall interactions, J Biomech Eng, 123 (2001), pp. 548-57.
- [9] A. QUANTERONI, L. FORMAGIA, Mathematical modelling and numeriacal simulation of the cardiovascular system in modelling of living system, Handbook of Numerical Analysis Series (P.G. Ciarlet, J.L. Lions Eds), Elsevier, Amsterdam, 2003.
- [10] M.J BARBARA, R.J. PETER, C. STUART, K. DAVID, Non-Newtonian blood flow in human right coronary arteries: steady state simulations. J Biomech, 37 (2004), pp. 709-720.
- [11] D.Y. FEI, J.D. THOMAS, S.E. RITTGERS, The effect of angle and flow rateupon hemodynamics in distal vascular graft anatomoses: a numerical model study. J Biomech Eng, 116 (1994), pp. 331-6.
- [12] M. Bonert, J. G. Myers, S. Fremes, J. Williams, C. R. Ethier, A Numerical Study of Blood Flow in Coronary Artery Bypass Graft Side-to-Side Anastomoses, Annals of Biomedical Engineering, 30(2002), pp. 599-611.
- [13] M-H. Song, M. Sato, Y. Ueda, Three-dimensional simulation of coronary artery bypass grafting with the use of computational fluid dynamics, Surg Today, 30 (2000), pp. 993-8.

Table II: Proposed and Actual Activity for Subproject 2.

Activity: Proposed (<->)	Months	Months	Months	Months	Months	Months
Actual (←→)	1-6	7-12	13-18	19-24	25-30	31-36
Construction of mathematical model.	<	>				
Development of numerical technique	<					
Design of numerical method (NM)						
Implementation of NM in a computer			-			
3. Validation • Design of schemes &			<			<u> </u>
analysis Computation & analysis						

Outputs of Subproject 2

Papers appeared/accepted in international journals	1
Papers presented in international conferences	2
Ph.D. graduates	2

Subproject 3: Mathematical Modeling of Disease Transmission

Principal Investigator: Prof. Dr. I. Ming Tang

The project commenced around the end of the first academic semester of 2002. As a program director in the Institute of Science & Technology for Research & Development, Mahidol University, the investigator of this subproject met on a regular basis with the program directors of the Center for Vaccine Development (CVD) and the Conservation Biology Center (CVB). Through his acquaintance with Prof. Sutee of CVD, he met with the French scientists at the Institute Recherche pour Development (IRD) who were working on the transmission of infectious diseases in Thailand. Dr. Tang established very close collaboration with them, especially Dr. Phillippe Barbazan. Dr. Barbazan served as the co-advisor to three of Dr. Tang's Ph.D. students, who have subsequently graduated with their Ph.D. They are now working at three universities in Thailand.

Due to the interests of the investigator's collaborators, he has worked on the following diseases:

- 1. Dengue Fever
- Malaria
- 3. West Nile Virus
- 4. Japanese Encepthalitis
- 5. Tuberculosis
- 6. Severe acute respiratory syndrome (SARS)
- 7. Leptosprosis
- 8. Smallpox

and has published papers on these diseases. Please see Appendices # 3.1-3.14 for full papers.

To further improve the research capabilities of the students, Dr. Tang have joined up with Dr. Phillippe Barbazan to set up a Franco-Thai Collabrative Research network involving six institutions and three units in France. We have been informed that our proposal (one of fifteen accepted) has been accepted and it is now running. This is a four year proposal. The title of the proposal is Spatial approach and mathematical modeling of emerging infectious diseases transmission and development of resistance. It is under the Franco – Thai Cooperation Program in Higher Education and Research. My team is only interested in that part of the proposal that is underlined.

Several officials in the Ministry of Public Health have indicated interests in the net-work of local surveillance centers in the provinces. Dr. Suwich Thammapalo, Chief, Dengue Fever Control Section, Bureau of Vector Borne Disease Control, MOPH is interested in my proposed network. Professor Dr. Virasakdi Chonsuvivatwong, Epidemiology Unit, Faculty of Medicine, Prince of Songkla University, who is the Ph.D. thesis advisor of Dr. Suwich is interested in the work of Dr. Puntani Pongsumpun. Dr. Suwich is working on a statistical model to correlate the data on the DHF cases, rain fall, rain days, max. and min. temp. and humidity in the monthly records over the past 20 years (1977-1997). Dr. Viroj Tangcharoensathien, Director of IHPP-Thailand, MOPH is working on projecting the HIV/AIDS incidences in different population groups in Thailand over the next forty years to help in determining the public health policies on AIDS from an economic viewpoint. The output of our work could assist the MOPH.

The MOPH are interested in our proposed network because it will be based in the provinces and not in Bangkok. This being the reason we recruited the students from the Rajabhat Institutes. The undergraduate students at these institutes are from the local villages in the provinces. They would return to the local villages and become teachers at the tamboon schools. They might be able to get the local people interested in public health issues of direct concern to them. Leptosprosis is a disease affecting the poorer provinces in Thailand where the medical care is not as advanced as in Bangkok and the other big cities. Having local people as part of a community-based public health surveillance units fits into the governmental plan of getting local people involved in thier own development.

Leptosprosis is also being used as the bacterium to determine the toxicity of nanoparticles, a project being undertaken in the Capacity Building Unit in Nanoscience & Nanotechnology of the Faculty of Science. This unit is also being headed by Prof. Dr Tang.

Table III: Proposed and Actual Activity for Subproject 3.

Activity: Proposed (Months	Months	Months	Months	Months	Months
Actual (\longleftrightarrow)	1-6	7-12	13-18	19-24	25-30	31-36
1. Modelling transmission of	<				***************************************	
dengue hemorrhagic fever.	←		,			>
2. Modelling cannibalism in an						
age structured predator-prey system.	<	>				
3. Modelling P. falcipurum			<u> </u>			
malaria transmission.				├		
4. Modelling of P. vivax malaria transmission.						
5. Analysis of feedback control			*	******************************	***************************************	***************************************
of blood platelet regulation by						
TPO.						
6. Study EPO regulation of				*		
erythrocytes production.						
7. Model the spread of seeds in tropical forests.				<u> </u>		

^{*} The investigator has become interested in SARs, Leptosporosis, and other diseases instead.

Outputs of Subproject 3

Papers appeared/accepted in international journals	14
Papers presented in international conferences	3
Ph.D. graduates	4
Master graduates	9

Subproject 4: Application of Log-linear and Logistic Models to Cancer Patients: A Case Study of the National Cancer Institute

Principal Investigator: Assoc. Prof. Dr. Montip Tiensuwan

The activities in this subproject have followed the proposed plan, that is,

- (1) Application of log-linear models to cancer patients: a case study of data from the National Cancer Institute.
- (2) Application of logistic regression models to cancer patients: a case study of data from the National Cancer Institute.

We finished number (1) and submitted our paper to the Southeast Asian Journal of Tropical Medicine and Public Health (see the manuscript in Appendix 4.1).

For number (2), application of logistic regression models, the aims of the study are as follows:

- 1. To analyze the cancer data by using logistic regression models to identify factors associated with the status of last contact of all cancer patients and estimate parameters of the models which indicate association between cancer variables.
- 2. To analyze the cancer data by using logistic regression models to identify factors associated with the status of last contact of cancer patients for individual gender and estimate parameters of the models which indicate association between cancer variables.
- 3. To analyze the cancer data by using logistic regression models to identify factors associated with the status of last contact of cancer patients for the specific site and estimate parameters of the models which indicate association between cancer variables.

Results of the completed study

The subjects were cancer patients treated at the National Cancer Institute. We collected cancer data by using a cancer notification form of the National Cancer Institute. The classification and coding of primary site and morphology are given in cancer notification form, that is ICD-O (9). This data set includes the number of new cancer patients who were admitted between January 2000 and December 2001 at the National

Cancer Institute. In this data set, there were 5,946 cancer patients which consisted of 2,042 male patients and 3,904 female patients.

The cancer data were considered according to the sex of cancer patients: male patients and female patients. In addition, each sex was classified into two parts as follows:

Part I Personal data. This part consists of age, region, marital status, race and religion.

Part II Cancer/clinical data. Factors being important variables in this part were as follows: Diagnostic evidence, site of cancer, pathological, stage of diagnosis, sites of metastasis, treatment which consists of surgery, radiation, chemotherapy, hormone and support and status of last contact.

Summary of general data of most patients

Part I: personal data. More patients were females than males. The majority of male patients ranges from 56 to 65 years of age, while female patients ranges from 46 to 55 years of age. We found that many of the patients were middle aged. Most of the patients were of Thai race, Buddhist religion, married / divorced / widowed patients and lived in the central part of Thailand.

Part II: cancer/clinical data. Most patients were diagnosed by using the histology of primary. A large number of female patients had cancer at their breasts and female genital organs, whereas, digestive organs were the positions at which cancer occurred most often for male patients. The majority of male patients had squamous cell neoplasms, while female patients had ductal, lobular and medullary neoplasms. Most patients were in the direct extension stage. Since more male patients were in the distant metastasis stage than female patients, more male patients had the sites of metastasis than the female patients. For treatments, radiation, surgery and chemotherapy, by order of preference, were used in male patients. While female patients were treated by surgery, radiation and chemotherapy, by order of preference. Most of patients survived with cancer.

Model for all cancer patients

The best logistic regression model to identify factors associated with the status of last contact for all cancer patients is given by the following equation:

$$\begin{aligned} \log \mathrm{it}(\hat{\pi}) &= -3.477 + 0.557X1 - 0.030X9 - 2.082X10 - 0.113X18 + 0.209X19 - 2.124X20 \\ &- 0.784X21 - 1.229X22 - 0.891X23 + 0.559X36 + 1.429X37 + 0.101X38 + \\ &- 0.511X39 - 0.615X40 + 1.424X41 + 1.06X42 - 0.677X44 + 2.001X47 - \\ &- 1.755(X18 \times X47) - 1.360(X19 \times X47) + 1.462(X20 \times X47) + 0.162(X21 \times X47) - 6.936(X22 \times X47) + 0.133(X23 \times X47). \end{aligned}$$

According to this model, the factors which effect the status of last contact are sex $\{X1\}$, marital status $\{X9, X10\}$, site of cancer $\{X18 - X23\}$, sites of metastasis $\{X36 - X42\}$, radiation $\{X44\}$, support $\{X47\}$ and site of cancer \times support $\{(X18 - X23) \times X47\}$.

Model for male cancer patients

By using the logistic regression models, the best model for male cancer patients that identify factors associated with the status of last contact is given by the equation below.

$$logit(\hat{\pi}) = -2.939 + 0.546X8 - 1.472X9 + 0.107X16 + 0.760X17 - 1.013X18 - 0.923X19$$
$$-1.450X39 - 0.842X40 + 1.661(X39 \times X40).$$

According to the above model, the factors which effect the status of last contact are marital status $\{X8, X9\}$, site of cancer $\{X16 - X19\}$, radiation $\{X39\}$, chemotherapy $\{X40\}$ and radiation \times chemotherapy $\{X39 \times X40\}$.

Model for female cancer patients

The best logistic regression model to identify factors associated with the status of last contact for female cancer patients is given by the following equation.

$$\begin{aligned} \log &\mathrm{it}(\hat{\pi}) = & -11.030 + 0.009\mathrm{X1} - 0.438\mathrm{X14} + 0.095\mathrm{X15} - & 2.343\mathrm{X16} - 0.634\mathrm{X17} - \\ & 0.244\mathrm{X18} + 6.026\mathrm{X25} + 8.594\mathrm{X26} + 5.731\mathrm{X27} + 0.428\mathrm{X28} + 7.583\mathrm{X37} + \\ & 3.072\mathrm{X38} - 1.712(\mathrm{X14} \times \mathrm{X38}) - 12.126(\mathrm{X15} \times \mathrm{X38}) + 1.327(\mathrm{X16} \times \mathrm{X38}) - \\ & 1.074(\mathrm{X17} \times \mathrm{X38}) - 0.802(\mathrm{X18} \times \mathrm{X38}) - 7.538(\mathrm{X25} \times \mathrm{X37}) - 6.276(\mathrm{X26} \times \mathrm{X37}) - 7.109(\mathrm{X27} \times \mathrm{X37}) + 0.744(\mathrm{X28} \times \mathrm{X37}) + 0.007(\mathrm{X1} \times \mathrm{X25}) - \\ & 0.043(\mathrm{X1} \times \mathrm{X26}) + 0.041(\mathrm{X1} \times \mathrm{X27}) - 0.027(\mathrm{X1} \times \mathrm{X28}) - 10.034(\mathrm{X37} \times \mathrm{X38}). \end{aligned}$$

According to the above model, the factors which effect the status of last contact are age $\{X1\}$, site of cancer $\{X14 - X18\}$, stage of diagnosis (extent) $\{X25 - X28\}$, chemotherapy $\{X37\}$, support $\{X38\}$, age × stage of diagnosis (extent) $\{X1 \times (X25 - X28)\}$, site of cancer × support $\{(X14 - X18) \times X38\}$, stage of diagnosis (extent) × chemotherapy $\{(X25 - X28) \times X37\}$ and chemotherapy × support $\{X37 \times X38\}$.

Models for the specific site in cancer patients

We classified the specific sites in cancer patients into five groups.

Group 1: Lip, oral cavity and pharynx

Group 2: Digestive organs

Group 3: Respiratory system and intrathoracic organs

Group 4: Female breast and female genital organs

Group 5: Thyroid gland, endocrine glands, eye, brain, central nervous system, lymph nodes, skin, blood, connective tissue, urinary tract, peritoneum and bones.

Model for Group 1

By using the logistic regression models, the best model for the patients who have cancer sites classified in this group, identifying factors associated with the status of last contact, is given by the equation below:

$$logit(\hat{\pi}) = -3.609 + 2.310X15$$

According to the above model, the factor which effects the status of last contact is support {X15}.

Model for Group 2

The best model for the patients who have cancer sites classified in this group identifying factors associated with the status of last contact is given by the following equation:

$$logit(\hat{\pi}) = -3.648 + 0.925X1 + 1.218X26 + 0.204X27 - 0.404X28 - 0.529X29 + 1.945X30 + 0.466X31$$

According to this model, the factors which effect the status of last contact are sex {X1} and sites of metastasis {X26 - X31}.

Using the logistic regression models with the dependent variable being the status of last contact, for the male patients who have cancer sites in this group, the best model is given by the following equation.

$$logit(\hat{\pi}) = -2.400 - 0.950X31$$

According to the above model, the factor which effects the status of last contact is chemotherapy {X31}.

Model for Group 3

For the patients who have cancer sites classified in this group, the best logistic regression model to identify factors associated with the status of last contact is given by the following equation:

$$\begin{aligned} \log &\mathrm{it}(\hat{\pi}) = -3.631 + 0.940 \mathrm{X}18 + 2.083 \mathrm{X}19 + 3.120 \mathrm{X}20 + 1.362 \mathrm{X}21 + 0.197 \mathrm{X}22 + \\ &1.028 \mathrm{X}23 + 2.378 \mathrm{X}24 + 2.650 \mathrm{X}28 - 2.444 (\mathrm{X}18 \times \mathrm{X}28) - 2.489 (\mathrm{X}19 \times \mathrm{X}28) - \\ &9.341 (\mathrm{X}20 \times \mathrm{X}28) - 2.779 (\mathrm{X}21 \times \mathrm{X}28) - 6.418 (\mathrm{X}22 \times \mathrm{X}28) - 2.127 (\mathrm{X}23 \times \mathrm{X}28) \\ &- 2.784 (\mathrm{X}24 \times \mathrm{X}28) \end{aligned}$$

According to the above model, the factors which effect the status of last contact are sites of metastasis $\{X18 - X24\}$, support $\{X28\}$ and sites of metastasis \times support $\{(X18 - X24) \times X28\}$.

Model for Group 4

By using the logistic regression models, the best model for the female patients who have cancer sites classified in this group that identify factors associated with the status of last contact is given by the equation below:

$$logit(\hat{\pi}) = -6.630 + 1.708X17 + 1.459X18 + 3.273X19 + 2.205X27$$

According to the above model, the factors which effect the status of last contact are stage of diagnosis (extent) {X17 - X19} and support {X27}.

Model for Group 5

For the patients who have cancer sites classified in this group, the best logistic regression models to identify factors associated with the status of last contact is given by the following equation:

$$logit(\hat{\pi}) = -3.647 - 0.025X1 - 1.844X24 + 1.764X25 - 17.490X26 + 0.325(X1 \times X26)$$

According to this model, the factors which effect the status of last contact are age $\{X1\}$, radiation $\{X24\}$, chemotherapy $\{X25\}$, support $\{X26\}$ and age \times support $\{X1 \times X26\}$.

In all the best models, the fitted value of each model is $\hat{\pi} = \frac{e^{\log it(\hat{\pi})}}{1 + e^{\log it(\hat{\pi})}}$.